Biogeosciences

Open Access

EGU

Nitrous oxide (N₂O) in Macquarie Harbour, Tasmania

Johnathan Daniel Maxey[1,2], **Neil D. Hartstein**[2], **Hermann W. Bange**[3], and **Moritz Müller**[1]

[1]Faculty of Engineering, Computing and Science, Swinburne University of Technology, Kuching 93350, Malaysia
[2]ADS Environmental Services, Kota Kinabalu, Sabah 88400, Malaysia
[3]Marine Biogeochemistry, GEOMAR Helmholtz Centre for Ocean Research Kiel, Wischhofstr. 1–3, 24148 Kiel, Germany

Correspondence: Johnathan Daniel Maxey (jdanielmaxey@gmail.com)

Abstract. Fjord-like estuaries are hotspots of biogeochemical cycling due to their steep physicochemical gradients. The spatiotemporal distribution of nitrous oxide (N₂O) within many of these systems is poorly described, especially in the Southern Hemisphere. The goals of this study are to describe the spatiotemporal distribution of N₂O within a Southern Hemisphere fjord-like estuary, the main environmental drivers of this distribution, the air–sea flux of N₂O, and the main drivers of N₂O production. Sampling surveys were undertaken in Macquarie Harbour, Tasmania, to capture N₂O concentrations and water column physicochemical profiles in winter (July 2022), spring (October 2022), summer (February 2023), and autumn (April 2023). N₂O samples were collected from middle water depths in the ocean (5 m), minor river (1 m) endmembers, the major river (10 m) endmember at 2 m from the bottom, and at five depths through the water column at four stations within the main harbour body.

Results indicate that N₂O was consistently supersaturated (reaching 170 % saturation) below the system's freshwater lens where oxygen concentrations are often hypoxic but infrequently anoxic. In the surface lens, levels of N₂O saturation vary with estimated river flow and with proximity to the system's main freshwater endmember. The linear relationship between apparent oxygen utilisation and ΔN₂O saturation indicates that nitrification is the process generating N₂O in the system. When river flow was high (July and October 2022), surface water N₂O was undersaturated (as low as 70 %) throughout most of the harbour.

When river flow was low (February and April 2023) N₂O was observed to be supersaturated at most stations. Calculated air–sea fluxes of N₂O indicated that the system is generally a source of N₂O to the atmosphere under weak river flow conditions and a sink during strong river flow conditions. The diapycnal flux was a minor contributor to surface water N₂O concentrations, and sub-halocline N₂O is intercepted by the riverine surface lens and transported out of the system to the ocean during strong river flow conditions. In a changing climate, western Tasmania is expected to receive higher winter rainfall and lower summer rainfall, which may augment the source and sink dynamics of this system by enhancing the summer and autumn efflux of N₂O to the atmosphere.

This study is the first to report observations of N₂O distribution, generation processes, and estimated diapycnal and surface N₂O fluxes from this system.

1 Introduction

Despite the fact that fjords and fjord-like estuaries represent only a small portion of the coastal area worldwide, they are responsible for sequestering 11 % of the global organic carbon (C) burial along terrestrial margins (Smith et al., 2015; Bianchi et al., 2018, 2020). These systems are significant sources of greenhouse gases (GHGs) to the atmosphere (Wilson et al., 2020; Rosentreter et al., 2023; Bange et al., 2024). Many are heavily stratified with strong water column physicochemical gradients (Acuña-González et al., 2006; Inall and Gillibrand, 2010; Hartstein et al., 2019; Salamena et al., 2021, 2022; Maxey et al., 2022). These gradients can be influenced by mesoscale climate drivers like the North Atlantic Oscillation (NAO) and Southern Annular Mode (SAM; see Austin and Inall, 2002; Gillibrand et al., 2005; Maxey et al., 2022) and local-scale drivers like freshwater input and marine intrusions (Inall and Gillibrand, 2010; Hartstein et al., 2019; Maxey et al., 2020; Salamena et al., 2022).

Nitrous oxide (N$_2$O) is a potent greenhouse gas (GHG), the increased presence of which in the atmosphere is primarily driven by emissions from agricultural soils (Tian et al., 2020, 2023). With a global warming potential nearly 300 times that of CO$_2$, N$_2$O is a key focus of climate studies (Myhre et al., 2013; Etminan et al., 2016; Eyring et al., 2021; Forster et al., 2021). Biological N$_2$O production occurs through the microbially mediated processes of ammonia oxidation, nitrite (NO$_2^-$) reduction, and nitrate (NO$_3^-$) reduction (Kuypers et al., 2018). In marine systems, N$_2$O production is influenced by environmental conditions such as dissolved oxygen (DO) availability, inorganic nitrogen (N) availability, light availability, temperature (e.g. Raes et al., 2016), pH (e.g. Breider et al., 2019), and microbial community composition (e.g. Wu et al., 2020). Many coastal systems are experiencing a reduction in DO availability (Limburg et al., 2020; Testa et al., 2023) and an increased presence of N$_2$O as a consequence (Laffoley and Baxter, 2019; Ji et al., 2020; Wilson et al., 2020; Wan et al., 2022; Orif et al., 2023; Resplandy et al., 2024).

Estuarine systems often have disproportionately high biological productivity relative to other marine systems (Walinsky et al., 2009; Gilbert et al., 2010; Bianchi et al., 2018, 2020). This also applies to N$_2$O dynamics, with approx. 33 % of marine N$_2$O emissions coming from estuaries (Bange et al., 1996; Seitzinger et al., 2000; Murray et al., 2015; Reading, 2022; Rosentreter et al., 2023). Estuaries can act as net sinks (Maher et al., 2016; Wells et al., 2018) or sources (De Bie, 2002; Zhang et al., 2010; Sánchez-Rodríguez et al., 2022) of N$_2$O depending on physical drivers of air–sea fluxes including waterbody and atmospheric concentration gradients, current velocities, depth, and wind speed (Wells et al., 2018; Bange et al., 2019). Other factors include land use modification (Reading et al., 2020; J. Chen et al., 2022) and the presence of microplastics (C. Chen et al., 2022). Despite the advancements made thus far, our understanding of marine N$_2$O distribution and atmospheric emissions is poorly constrained and needs improvement (Bange et al., 2019, 2024), especially in Southern Hemisphere fjord-like systems (Yevenes et al., 2017). Much of the current uncertainty lies with a lack of in situ data describing seasonal N$_2$O dynamics being available to constrain global emission models (Bange et al., 2019).

The purpose of this study was (1) to investigate the distribution and seasonal variability in N$_2$O concentrations and emissions in a Southern Hemisphere fjord-like estuary and (2) to decipher the major physical and biological drivers of these emissions.

2　Methods

2.1　Study area

Macquarie Harbour is a Southern Hemisphere fjord-like estuary located on the western coast of Tasmania, Australia (Fig. 1). The harbour is oriented NW–SE and is approximately 33 km long, 9 km wide, and has a surface area of 276 km^2. The mouth of the harbour is constricted by a shallow (4–8 m) and long (14 km) sill known as "Hells Gates". Hells Gates muffles tidal forcing, resulting in harbour water levels primarily determined by the river flow and wind set-up (Hartstein et al., 2019). The morphology of this system results in sharp gradients of DO, salinity, and temperature that are seasonally dependent (Cresswell et al., 1989; Hartstein et al., 2019; Maxey et al., 2022). In surface waters, dissolved oxygen (DO) concentrations are nearly always in equilibrium with the air but decrease sharply through the halocline ($\sim$ 8 to 15 m). There is almost no DO produced below the halocline (8 to 12 m deep) due to high chromophoric dissolved organic matter (CDOM) levels limiting primary production at the surface (Maxey et al., 2017, 2020). Sub-halocline layers ($\sim$ 15 m to a few metres from the bottom) are observed to have DO concentrations below 62.5 μM more than 50 % of the time (see Maxey et al., 2022). Near the seabed, episodic marine intrusions (deep-water renewal) refresh the supply of DO near the mouth of the system but refresh the upper reaches of the harbour less frequently (see Andrewartha and Wild-Allen, 2017; Hartstein et al., 2019; Maxey et al., 2022). This process is driven by low atmospheric pressure, sustained NW winds, and low catchment rainfall, which itself is influenced by the Southern Annular Mode (SAM) (Hartstein et al., 2019; Maxey et al., 2022). In the harbour's upper reaches, DO concentrations fall below 31 μM nearly a third of the time (Maxey et al., 2022). Hydrodynamic and oxygen tracer numerical model simulations of the harbour by Andrewartha and Wild-Allen (2017) estimate that 50 % of the harbour's basin waters are replaced every 65 d during low-river-flow conditions and approximately 110 d during normal flow conditions.

The main source of freshwater to the harbour is located on its southeast end (the Gordon River) and drains a nearly pristine catchment (including the Franklin River) of approximately 5682 km^2 (Macquarie Harbour Dissolved Oxygen Working Group, 2014; Fig. 1). The Gordon River discharges an estimated 180 000 t organic carbon (OC) per year into the estuary (Maxey et al., 2020, 2022). It should be noted that this area receives the some of the highest rainfall (more than 2500 mm yr^{-1}) volume in Australia (Dey et al., 2019). The King River, located on the harbour's northern end, is the second-largest contributor of fresh water to the estuary and drains a catchment area of 802 km^2. Unlike the Gordon River, the King River has a history of receiving treated mining (e.g. copper) effluent and transporting this to the harbour (Carpenter et al., 1991; Teasdale et al., 2003).
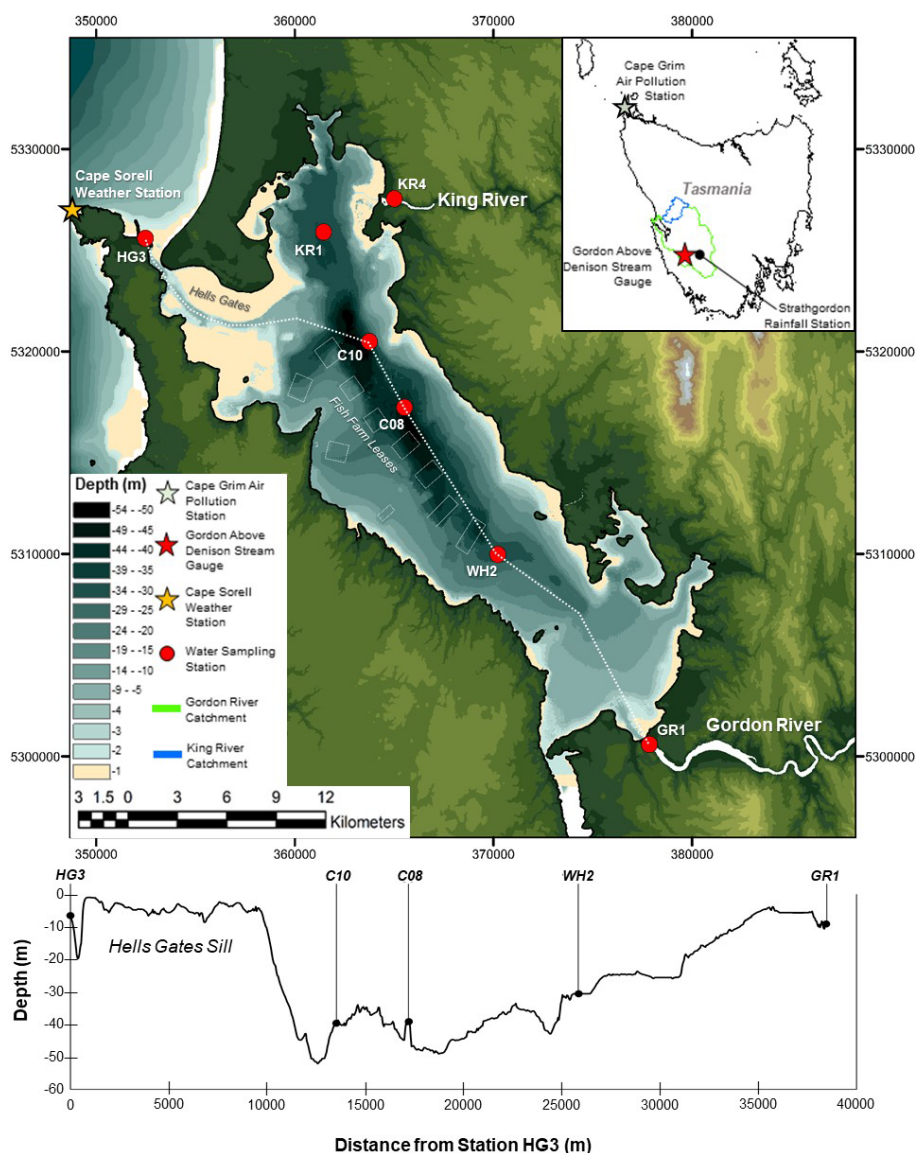
Figure 1. Macquarie Harbour, Tasmania. Water sampling stations are shown with red circles. The Kennaook / Cape Grim Air Pollution monitoring station is shown as a green star (see inset map). Cape Sorell Weather Station shown as an orange star. The Gordon Above Denison Stream Gauge is shown as a red star (see inset map). Aquaculture lease boundaries are shown as hollow rectangles. Lease locations are sourced from Land Information Systems Tasmania (LISTmap – https://maps.thelist.tas.gov.au/ last access: 1 November 2024). Station names reflect general harbour locations, where KR1 indicates King River 1; C10 and C08 indicate Central Harbour 10 and 08, respectively; WH2 indicates World Heritage Area 2; and GR1 indicates Gordon River station 1. Coordinates are displayed in GDA_1994_MGA_Zone_55 format. Bathymetry through the system is shown as a dashed line. Note that this track excludes stations KR4 and KR1.

2.2 Experimental design

Nitrous oxide distribution was assessed by collecting water samples across seven stations, including the harbour's end-members (the mouths of the Gordon and King rivers and the harbour mouth at Hells Gates Inlet; see Fig. 1 and Table 1) and stations along the longitudinal axis of the harbour where the deepest basins are located (named KR1, C10, C08, and WH2). Samples collected at endmember stations were collected from a single depth as these stations are shallow. Sam-

ples in the harbour body were collected at five depths from the surface (2 m) to approx. 1 m from the seabed. Collection campaigns were conducted in July 2022, October 2022, February 2023, and April 2023. At each station and depth, three replicate vials ($n = 3$) were collected for the determination of N$_2$O concentration.

2.3　Field sampling

At each station, water quality sonde profiles were collected from the surface to the seabed at 1 m intervals using a YSI EXO-1 equipped with optical DO (accuracy from 0 to 625 μM ±3 μM or 1 % of the reading, whichever is greater; precision is 0.03 μM), salinity (accuracy ±0.1 % or 1 % of the reading, whichever is greater; precision is 0.01), temperature (accuracy is ±0.15 °C, and precision is 0.01 °C), and depth sensors. Sonde calibration was checked and corrected (when needed) for each sampling period.

Water samples were collected at various depths (see Table 1) using a 5 L Niskin bottle sampler. Water sample parameters include dissolved total ammoniacal N (NH$_3$+ NH$_4^+$) (TAN), NO$_3^-$, and N$_2$O. N$_2$O samples were collected in triplicate immediately after retrieval of the Niskin bottle by transferring water from the bottle through silicone tubing into a 20 mL borosilicate vial. Sample water was added to the vial by placing the tubing at the bottom and allowing the vial to overflow several volumes before sealing with a butyl rubber stopper and aluminium crimp. After ensuring the sample vial was free of bubbles, 50 μL of saturated mercury chloride (HgCl$_2$) solution was injected into the sample to arrest biological activity. All N$_2$O samples were shipped to GEOMAR in Kiel, Germany, for analysis. Samples were measured in July and August 2023 within 4 to 12 months after sampling and were not affected by the storage time (Wilson et al., 2018).

Water collected for dissolved inorganic N was filtered immediately using 0.45 μm polyethersulfone syringe filters (Whatman Puradisc). Samples were stored in a chilled dark container until being transported to Analytical Services Tasmania in Hobart, Australia, for analysis. Dissolved total TAN and NO$_3^-$ were analysed using a Lachat Flow Injection Analyser. TAN and NO$_3^-$ analyses used methods based on APHA standard methods (2005) 4500-NH$_3$ H (reporting limit 0.005 mg L^{-1}) and 4500-NO$_3^-$ L^{-1} (reporting limit 0.002 mg L^{-1}).

2.4　Analysis of rainfall and river loading estimation

Rainfall and river discharge were analysed using methods presented in Maxey et al. (2022), where rainfall and stream gauge data were collected from the Gordon River catchment, the Strathgordon Rainfall Gauge Station and the Gordon Above Denison (GAD) Stream Gauge (Fig. 1). The rainfall and flow metrics computed include the average daily rainfall over a 20 d period prior to sampling; total accumulated rainfall 20, 10, 5, and 3 d prior to sampling; estimated Gordon River flow into the estuary; and measured flow at the GAD Stream Gauge.

Gordon River flow was estimated by scaling daily rainfall to the size of the catchment and assuming a rainfall and runoff coefficient of 0.70 adopted from a neighbouring catchment with similar land cover, geology, and slope (Willis,

2008). Additional streamflow from Gordon River dam releases was estimated by subtracting scaled rainfall contributions to river flow measured at the GAD Stream Gauge. This flow was added to the estimated runoff entering the harbour. Rainfall and flow data were provided by the Australian Bureau of Meteorology (BOM). NO$_3^-$ and TAN loading were estimated my multiplying the measured concentration of each parameter at station GR1 (see Fig. 1 and Table 1) by the estimated Gordon River flow.

2.5　Analysis of water column N$_2$O concentrations, air–sea flux, and diapycnal flux

2.5.1　Determination of N$_2$O concentrations

Water samples were analysed for N$_2$O using the static headspace equilibration method followed by gas chromatographic separation (HP Agilent 5890) and detection with an electron capture detector (ECD) as described in Bange et al., (2019), Bastian (2017), and Kallert (2017). The concentration of N$_2$O in the samples was calculated with the following equation (Eq. 1; see Bange, 2006):

$$C_{\mathrm{obs}} = \frac{x' P V_{\mathrm{hs}}}{RTPV_{\mathrm{wp}}} + X'\beta P. \tag{1}$$

C_{obs} is the concentration (nmol L^{-1}) of N$_2$O in the water sample; x' is the measured dry mole fraction of N$_2$O in the sample vial's headspace; P is the ambient pressure set to 1 atm; V_{hs} and V_{wp} are the volumes of the headspace in the vial and water in the vial, respectively; R is the gas constant; T is the temperature during equilibrium; and β is the solubility of N$_2$O (Weiss and Price, 1980). The mean relative error in the concentration values obtained was 2.4 % (±0.16).

2.5.2　Estimation of N$_2$O air–sea fluxes and N$_2$O saturations

N$_2$O air–sea fluxes (F in μmol m^{-2} d^{-1}) were estimated using equations from Zhang et al. (2010) and Bange et al. (2019) (Eq. 2):

$$F = K \times (C_{\mathrm{obs}} - C_{\mathrm{eq}}). \tag{2}$$

C_{obs} is the measured concentration (nmol L^{-1}) of N$_2$O in the water sample, while C_{eq} is the air-equilibrated seawater N$_2$O concentration calculated for in situ temperature and salinity using the solubility data of Weiss and Price (1980). K is the gas transfer velocity, which in the absence of direct measurements can be expressed as a function of the wind speed and the Schmidt Number (Sc). For this study we sourced daily average wind speed from the Cape Sorrel Weather Station at the northern end of Macquarie Harbour (http://www.bom.gov.au/climate/data/index.shtml, last access: 1 October 2024, station ID 097000; see Fig. 1 for the station location). K was estimated using relationships

Table 1. Sampling stations showing coordinates, parameters, and sampling depth for each parameter (in m).

Station	Station depth (m) (MSL)	Dissolved oxygen salinity temperature	N$_2$O	TAN (NH$_3$+ NH$_4^+$)	NO$_3^-$
HG3 352484, 5325594	8	Every metre	5 m	5 m	5 m
KR4 365018, 5327550	3	1 m	1 m	1 m	1 m
KR1 361316, 5325972	36	Every metre	2, 12, 20, 30, 35 m	2, 12, 20, 30, 35 m	2, 12, 20, 30, 35 m
C10 363708, 5320464	44	Every metre	2, 12, 20, 30, 42 m	2, 12, 20, 30, 42 m	2, 12, 20, 30, 42 m
C08 365489, 5317238	47	Every metre	2, 15, 25, 35, 45 m	2, 15, 25, 35, 45 m	2, 15, 25, 35, 45 m
WH2 370218, 5309894	32	Every metre	2, 12, 20, 25, 30 m	2, 12, 20, 25, 30 m	2, 12, 20, 25, 30 m
GR1 377784, 5300603	12	Every metre	10 m	10 m	10 m

in Nightingale et al. (2000), Raymond and Cole (2001), and Wanninkhof (2014). Fluxes at Macquarie Harbour's endmember stations used K values that account for additional forcings like bottom shear (see Raymond and Cole, 2001; Zappa et al., 2003; Abril and Borges, 2004; Beaulieu et al., 2012; Rosentreter et al., 2021). Deeper stations in the harbour's main body (i.e. KR1, C10, C08, WH2) have surface layers that are separated from the seabed by more than 10 m. Wind-based K_{600} estimators were used to estimate air–sea flux in those locations (see Nightingale et al., 2000; Raymond and Cole, 2001; Wanninkhof, 2014). Atmospheric N$_2$O for this estimation was sourced from monthly mean baseline greenhouse gas mole fractions measured at the Kennaook / Cape Grim Baseline Air Pollution Station, located in northwestern Tasmania. This station measures atmospheric N$_2$O using a gas chromatograph (GC) equipped with an ECD (https://www.csiro.au/en/research/natural-environment/atmosphere/latest-greenhouse-gas-data last access: 1 November 2024). N$_2$O saturation (in %) was computed as N$_2$O saturation $= 100 \times (C_{obs}/C_{eq})$.

2.5.3 Estimation of diapycnal N$_2$O flux

N$_2$O diapycnal fluxes (F_{dia}; Eq. 3) from basin waters (sample depths of 20 or 25 m) to the harbour's surface lens (sample depths of 2 m) were estimated as follows:

$$F_{dia} = K\rho \frac{d[N_2O]}{dz}, \qquad (3)$$

where z is depth. Diapycnal diffusivity (K_ρ; Eq. 4) is computed with the local buoyancy frequency (N^2), Γ is set to 0.2 (Osborn, 1980), and ε is the dissipation rate of turbulent kinetic energy assumed to be on the upper end of values for the mixing zone of stratified systems 1×10^{-5} (Arneborg et al., 2004; Mickett et al., 2004; Fer, 2006).

$$K_\rho = \Gamma \frac{\varepsilon}{N^2} \qquad (4)$$

2.6 Data analysis

The relationships between N$_2$O saturation and water quality parameters such as DO concentration, salinity, temperature, nitrate, and ammonium concentrations are determined using Pearson correlation. Differences in mean N$_2$O saturation between season, depth and each sampling station were tested using a two-way ANOVA. Differences between rainfall and river flow metrics between seasons were tested using one-way ANOVA, and pair-wise testing using Bonferroni's correction was undertaken where significant differences between seasons were detected. The relationship between rainfall and river flow metrics from the Gordon River and surface water N$_2$O saturation and N$_2$O air–sea flux at each station was analysed using the Pearson correlation. The standard deviation (SD) of the mean air–sea flux and diapycnal flux was computed from error propagated from replicate observations of N$_2$O wind speed, N$_2$O concentration, and density (where appropriate) using methods from Ku (1966). Contour plots were made with Plotly Chart Studio (Plotly Technologies Inc.) with the title "Collaborative data science" (Montréal, QC, Canada, 2015; https://plot.ly, last access: 1 November 2024).

3 Results

3.1 Rainfall and river loading

The 20 d rainfall accumulation ranged from a low of 117 mm in July 2022 to a high of 139 mm in April 2023 (see Fig. 2a). Average ($\pm$ se) daily rainfall was similar across all months and ranged from 5.12 (± 2.57) mm in July 2022 to 5.79 (± 3.03) mm in October 2022 (see Fig. 2b) with no seasonal differences detected ($p = 0.4326$).

Estimated flow at the Gordon River mouth and GAD stream gauge was greater in July and October 2022 than February and April 2023 (Fig. 2c). Significant seasonal differences in flow measured at the GAD stream gauge were detected ($p = 5.5 \times 10^{-7}$), with greatest flow in July and October 2022 and decreasing flow over February and April 2023. July flows at the GAD stream gauge were observed to be 107.6 (± 15.9) m^3 s^{-1} and in April 2023 were observed to be 30.5 (± 2.2) m^3 s^{-1} (Fig. 2d).

Estimated NO_3^- and TAN loading varied with NO_3^- loads of $1.69 \, t \, d^{-1}$ observed in July 2022, which then dipped to $0.31 \, t \, d^{-1}$ in October 2022 and then increased again to 1.77 and $2.77 \, t \, d^{-1}$ in February and April 2023 (Fig. 2e). TAN loading mirrored this pattern, with peaks occurring in October 2022 and February 2023 and lows occurring in July 2022 and April 2023. N_2O loading from the Gordon River was observed to be $0.015 \, t \, d^{-1}$ in July 2022, $0.012 \, t \, d^{-1}$ in October 2022, $0.015 \, t \, d^{-1}$ in February 2023, and $0.016 \, t \, d^{-1}$ in April 2023 (Fig. 2f).

3.2 Water column physicochemical profiles

DO profiles at the stations located within the main body of the harbour show a well-oxygenated surface layer that rapidly attenuates with depth (Fig. 3a) through the halocline (Fig. 3b). There is a prominent riverine surface lens in the main harbour extending to depths of up to 8 m depending on sampling period and location within the estuary. Salinity in the surface waters was lower in July and October 2022 (6 to 13) than February and April 2023 (greater than 20). Below the halocline, salinity ranged from approx. 28 to 32.

The DO gradient between the surface and sub-halocline waters was steeper in October relative to July 2022, with October 2022 DO concentrations approaching single digits ($3.1 \, \mu M$) at station WH2, which is the nearest station to the Gordon River mouth (see Fig. 1). In general, the sub-halocline concentrations of DO were lower with proximity to the Gordon River mouth. The temperature of the freshwater surface layer ranged from about 9 to 19 °C but showed little variation below the halocline where temperature ranged between 13 and 16 °C (Fig. 3c).

Nitrate concentrations in the surface water lens tended to be lower than those observed at sub-halocline depths (Fig. 4a). The greatest NO_3^- concentrations were observed 2 m above the seabed at station WH2 in July and October 2022 and at mid-basin depths at stations C10 and C08 during those same periods, with concentrations reaching $1.77 \, \mu mol$. TAN concentrations were often observed below detection limits ($0.3 \, \mu mol$) but were greatest in the surface lens or within the halocline itself when detectable (Fig. 4b). TAN concentrations at WH2 tended to be found at higher levels through the water column relative to other stations (down to about 20 m) reaching $1.53 \, \mu mol$ at 15 m in October.

3.3 N_2O distribution

At each harbour station, depth and season (and their interaction) significantly impacted N_2O saturation (two-way ANOVA, $\alpha = 0.05$, degree of freedom (d.f.) = 59). At 2 m, N_2O saturation was observed to be below 100 % at all stations in July 2022 (Figs. 5 and 6) and at stations KR1, C10, and C08 in October 2022. In February and April 2023, N_2O saturation in the harbour was above 100 % through the water column except in KR1 surface waters. The maximum N_2O

concentrations were observed in the sub-halocline. Among the sub-halocline observations, the maximum N_2O concentrations (reaching over 170 %) were observed at the base of the Hells Gates sill at station C10 in October 2022.

All endmember N_2O concentrations were undersaturated in July 2022. In October, stations KR1 and HG3 were observed to be approx. 100 % saturated, but N_2O at station GR1 was undersaturated. In February and April 2023, N_2O concentrations were supersaturated at all endmember stations. There were statistically significant linear correlations between N_2O saturation and salinity ($r = 0.494$; $p = 5.5 \times 10^{-7}$, $n = 92$), temperature ($r = 0.391$; $p = 1.2 \times 10^{-4}$; d.f. = 90), DO concentration ($r = -0.563$; $p = 5.2 \times 10^{-9}$; d.f. = 90), and nitrate concentration ($r = 0.559$; $p = 6.9 \times 10^{-9}$; d.f. = 90) in the harbour stations (Fig. 7). The correlation between N_2O saturation and the TAN concentration, however, was not statistically significant ($r = 0.174$; $p = 0.31$; d.f. = 34).

3.4 N_2O air–sea and diapycnal fluxes

Atmospheric N_2O mole fractions measured at Kinnaook / Cape Grim Air Pollution Station (see Fig. 1) were observed to increase from 334.7 ppb in July 2022 to 335.9 ppb in February 2023. The April 2023 atmospheric N_2O mole fraction was slightly lower than that observed in February 2023 at 335.6 ppb. Average ($\pm$ SD) wind speeds were observed to be 6.6 (± 3.7) $m \, s^{-1}$ in July, 5.6 (± 2.5) $m \, s^{-1}$ in October, 6.3 (± 3.4) $m \, s^{-1}$ in February, and 6.4 (± 4.0) $m \, s^{-1}$ in April.

Estimated N_2O air–sea flux in the main harbour stations (KR1, C10, C08, WH2) ranged from -12.88 (± 6.00) μmol $N_2O \, m^{-2} \, d^{-1}$ at C10 in July 2022 (negative sign indicates absorption of N_2O into the surface waters from the atmosphere) to 7.31 (± 3.43) $\mu mol \, N_2O \, m^{-2} \, d^{-1}$ at the same station in February 2023 (using the "high" K_{600} estimator from Raymond and Cole, 2001; see Table 2)

Station KR1 was always observed to be a site of atmospheric N_2O uptake and was every non-endmember station in July 2022. Near the head of the system, station WH2 was observed to be a net source of N_2O to the atmosphere from October 2022 to April 2023, and stations C10 and C08 (positioned above the deepest basins) were net sources in February 2023 and April 2023.

Estimated diapycnal fluxes ($\pm$ SD) using local buoyancy frequencies showed a consistent upwards movement of N_2O from the sub-halocline to surface layers, with the smallest fluxes observed in July 2022 ($49 \pm 2.3 \, nmol \, N_2O \, m^{-2} \, d^{-1}$ at C08), and the largest fluxes observed in October 2022 (up to $1308 \, nmol \, N_2O \, m^{-2} \, d^{-1}$ at WH2) and February 2023 (up to $1200 \pm 47.3 \, nmol \, N_2O \, m^{-2} \, d^{-1}$ at C10); see Table 3. Patterns in the size of the diapycnal flux generally reflected the patterns of N_2O % saturation, with the largest fluxes occurring in October 2022 during the periods of greatest N_2O %
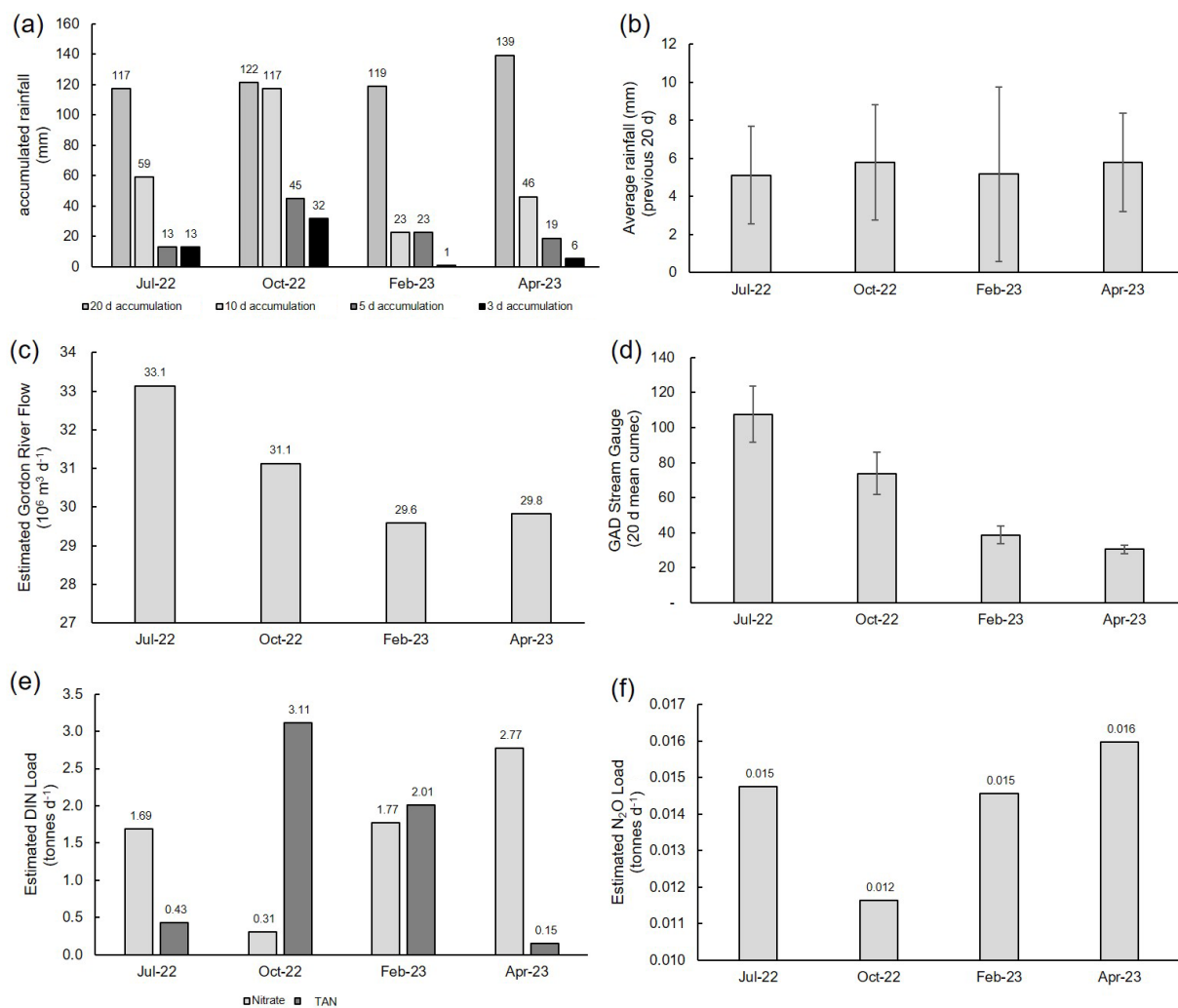
Figure 2. Rainfall and estimated Gordon River loading estimates for each sampling event: **(a)** accumulated rainfall (mm) 10, 5, and 3 d prior to each sampling event; **(b)** average (mean) daily rainfall over a 20 d period prior to each sampling event; **(c)** estimated Gordon River flow into the harbour in millions of cubic metres per day; **(d)** daily mean flow ($m^3 s^{-1}$) over the 20 d prior to sampling ($\pm$ standard error) at the Gordon Above Denison Stream Gauge; **(e)** estimated nitrate and ammonium loads entering the harbour from the Gordon River; and **(f)** estimated N₂O load ($t d^{-1}$) entering the harbour from the Gordon River.

saturation. Overall, the magnitude of the estimated diapycnal fluxes was smaller than estimated air–sea fluxes.

4 Discussion

Our study is the first to report on N₂O distribution and air–sea flux from an Australasian fjord-like estuary. We set out to investigate how N₂O concentrations varied along horizontal and depth gradients, how N₂O concentrations and estimated surface water emissions vary seasonally, how N₂O concentrations vary with freshwater inputs, and whether the relationship between apparent oxygen utilization (AOU) and ΔN_2O could help clarify the primary mechanism for N₂O generation in this system. We used surface water observations, local wind speed (from Cape Sorell weather station),

and atmospheric N₂O mole fractions (from Kennaook / Cape Grim; Fig. 1) to estimate N₂O air–sea flux (based on Zhang et al., 2010, and Bange et al., 2019) and found that Macquarie Harbour functions as both a site of atmospheric uptake and emission of N₂O. Most harbour stations were estimated to be removing atmospheric N₂O in July and October 2022 (when river flow was greater) and emitting N₂O into the atmosphere in February and April 2023 (during low-river-flow periods; see Fig. 8 and Table 2). Pearson correlations show that when freshwater flow is high, N₂O air–sea flux is negative (indicating uptake from the atmosphere), and when freshwater flow is low, N₂O air–sea flux is positive (Table 2). Our observations highlight that freshwater flow is a key driver of N₂O emissions in this estuary. In addition, Gordon River flow is heavily influenced by hydroelectric dam
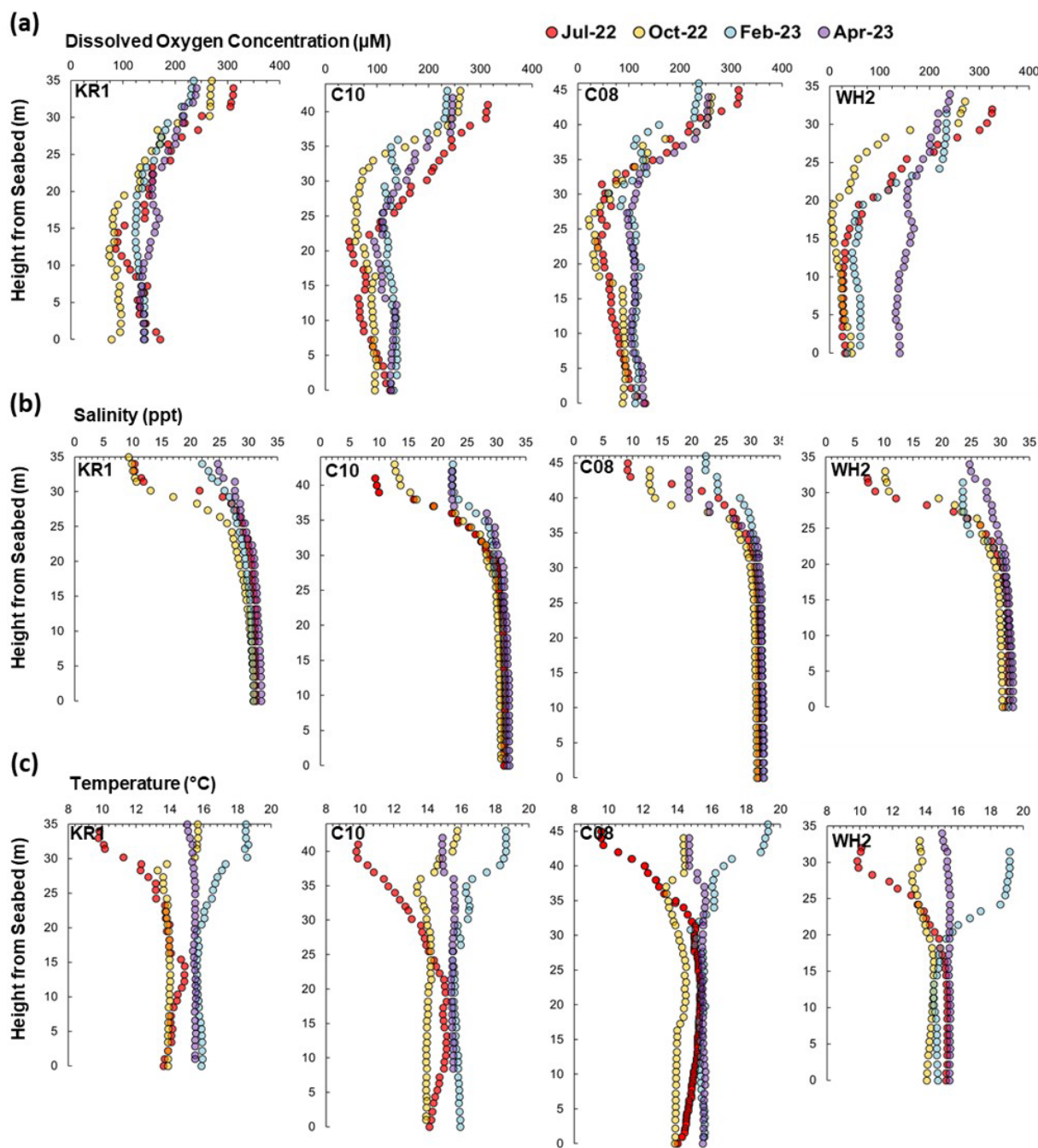
Figure 3. Dissolved oxygen (μM) **(a)**, salinity **(b)**, and temperature (°C) **(c)** profiles (referencing height from seabed) collected at stations KR1, C10, C08, and WH2 in July 2022 (red dots), October 2022 (yellow dots), February 2023 (blue dots), and April 2023 (purple dots). Measurements were made every 1 m.

release (up to ∼ 28 % of the flow in July 2023). Rainfall in the catchment area may offset the effects of dam release, but our observations did not capture this as rainfall itself was not significantly correlated with N_2O concentrations or air–sea flux.

The river endmember concentrations of N_2O were often observed to be undersaturated, as observed in the South Platte River basin, USA (McMahon and Dennehy, 1999); Neuse River estuary, USA (Stow et al., 2005); headwater streams in Ontario, Canada (Baulch et al., 2011); and Upper Mara River basin, Kenya (Mwanake et al., 2019). Our observations of river endmember N_2O concentrations were similar to the lower end of the concentrations reported in McMahon and Dennehy (1999) (approx. 80 % saturation) but not as low
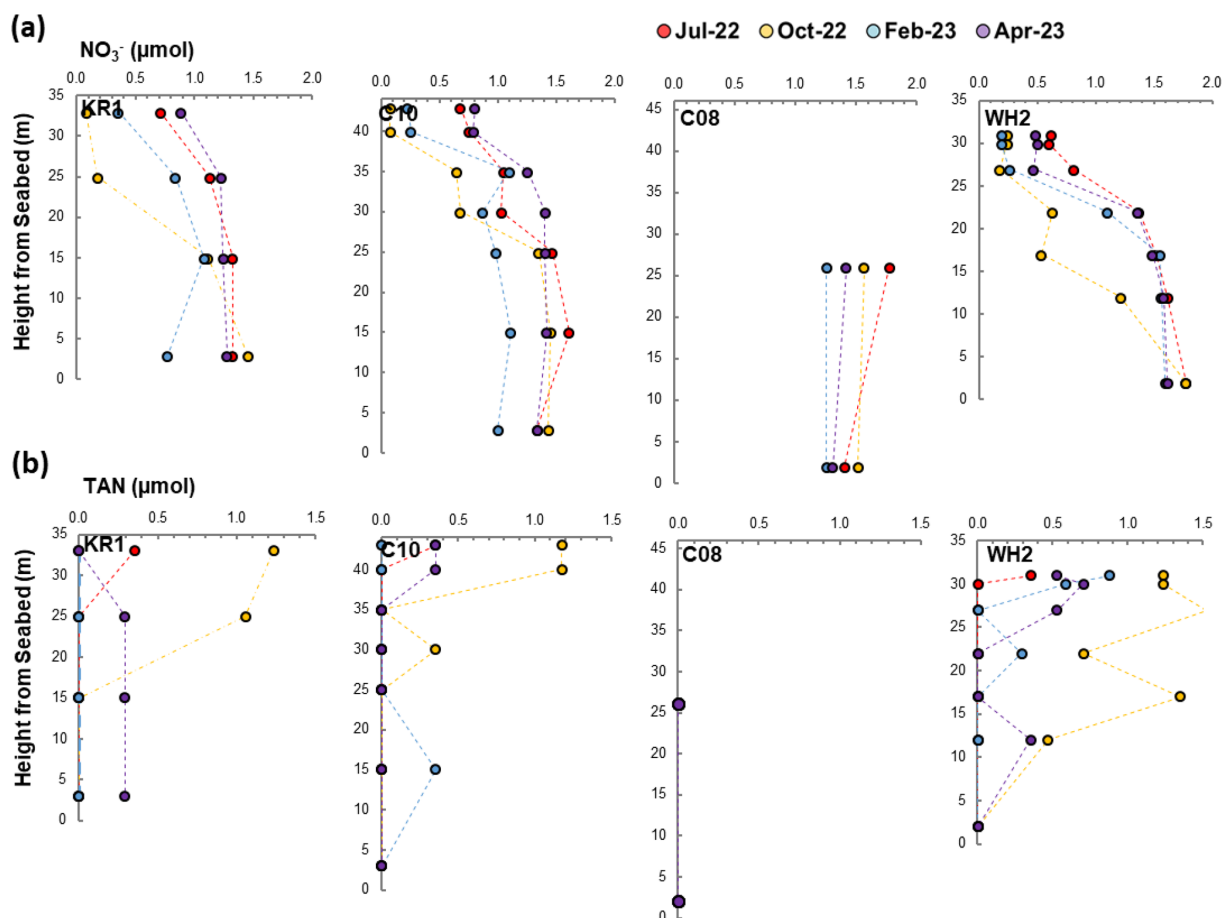
Figure 4. Nitrate NO$_3^-$ (**a**) and TAN (**b**) concentrations with depth (referencing height from seabed) collected at stations KR1, C10, C08, and WH2 in July 2022 (red dots), October 2022 (yellow dots), February 2023 (blue dots), and April 2023 (purple dots). Data presented as having a concentration of 0.0 are below the detection limits of the analyte.

as those reported Jackson Creek, Ontario, Canada, in Baulch et al. (2011), where some observations reached < 20 % saturation. N$_2$O undersaturation in those systems was attributed to complete denitrification (use of N$_2$O as a terminal electron acceptor by denitrifiers) in streams with high DOC loads, low DO, and low NO$_3^-$ concentrations. It should also be noted that up to 28 % of the estimated Gordon River flow was found to be associated with flow through the Gordon Above Denison Stream Gauge (a proxy for hydroelectric dam and reservoir release to the Gordon River). Boreal reservoirs have been shown to be net sinks of atmospheric N$_2$O (Hendzel et al., 2005), which was attributed to increased N$_2$O demand to drive complete denitrification. There is good reason to believe that N$_2$O may be scavenged in the Gordon and King rivers as well because they do often have high DOC concentrations, high water column DO demand (Maxey et al., 2020), and low DO concentrations near the stream bed (Maxey et al., 2022).

Below the estuary's predominately freshwater surface lens, the fjord-like morphology drives suboxic conditions like those observed in the sub-halocline waters at station WH2 in October 2022 (see Fig. 3; Hartstein et al., 2019; Maxey et al., 2020, 2022). While these conditions do not always persist, DO concentrations below 31 µM have been observed to occur more than 30 % of the time up the estuary, specifically at station WH2 (Maxey et al., 2022). In the low-DO sub-halocline layers of the harbour we observed the maximum N$_2$O concentrations (Figs. 5 and 6). Sub-halocline N$_2$O saturation was observed to generally range from approx. 110 % to 170 %, with the highest values observed within the deeper basins near the foot of the sill (stations C10 and C08; Fig. 6).

In the harbour's sub-halocline layer there is not enough light to support photosynthesis (Hartstein et al., 2019; Maxey et al., 2017, 2020, 2022), and thus the main source of oxygen is advection from marine intrusions. N$_2$O producing microbes have been observed to populate this layer of the harbour (see Da Silva et al., 2022), and our observations of supersaturated N$_2$O in these layers show that those microbes are active. Linear relationships between AOU and
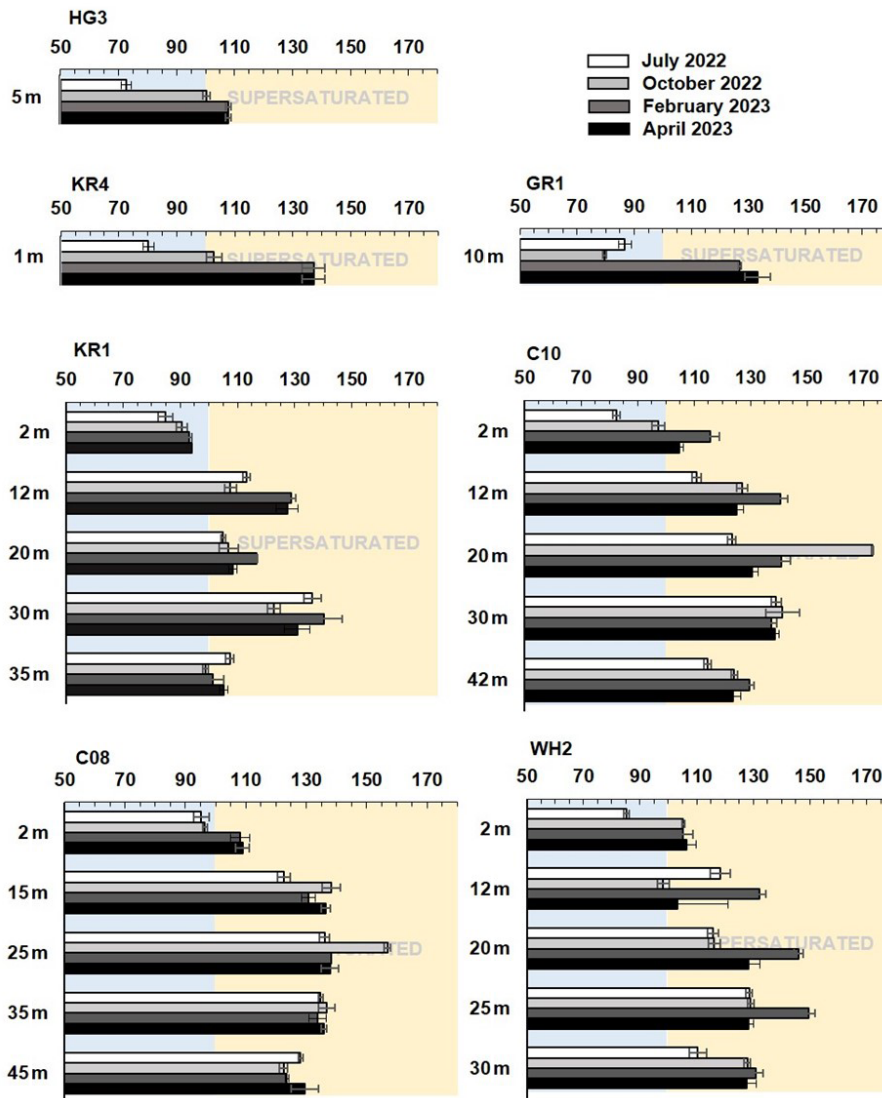
Figure 5. Mean ($\pm$ standard error) N$_2$O % saturation observed at each sampling station with depth and across seasons. Note that a dashed red line indicating 100 % at the time of sampling has been placed in each panel for reference.

ΔN$_2$O (slope $= 0.0154$; $r = 0.596$; $p = 2.4 \times 10^{-23}$; Fig. 7c) and NO$_3^-$ and N$_2$O saturation ($r = 0.559$; $p = 6.9 \times 10^{-9}$; Fig. 7d) indicate that N$_2$O production likely occurs primarily through the ammonia oxidation (nitrification) pathway (Yoshinari, 1976; Walter et al., 2004; Brase et al., 2017). Our observations are on the lower end of reported N$_2$O yield per mole O$_2$ consumed (see Suntharalingam and Sarmiento, 2000; Brase et al., 2017), which may be an artefact of mixing and loss dynamics such as basin water DO recharges from marine intrusions and loss to aerobic respiration and the atmosphere. This suggests that some portion of sub-halocline pelagic oxygen demand in the harbour can be attributed to nitrifying microbes (albeit at a much lower rate compared to aerobic respiration). Ji et al. (2020) also observed similar relationships in the Saanich Inlet, a seasonally anoxic fjord-like

estuary in British Columbia, but in that system anoxic conditions are more persistent (Bourbonnais et al., 2013; Manning et al., 2010) compared to Macquarie Harbour (Maxey et al., 2022). Deep-water renewal and marine intrusions have been hypothesised to stimulate N$_2$O production in the Saanich Inlet (Capelle et al., 2018; Michiles et al., 2019; Ji et al., 2020) and Baltic Sea (Walter et al., 2006) and may also be stimulating it in Macquarie Harbour as well. In the Baltic Sea, Walter et al. (2006) and Myllykangas et al. (2017) observed enhanced N$_2$O production in areas receiving significant marine intrusions. Positive correlations between AOU and ΔN$_2$O observed in western Baltic Sea waters (Walter et al., 2006), along with mean (11 years from 2006–2017) seasonal variations in DO and N$_2$O observed through the water column at the Boknis Eck Time Series Station (Eckernförde
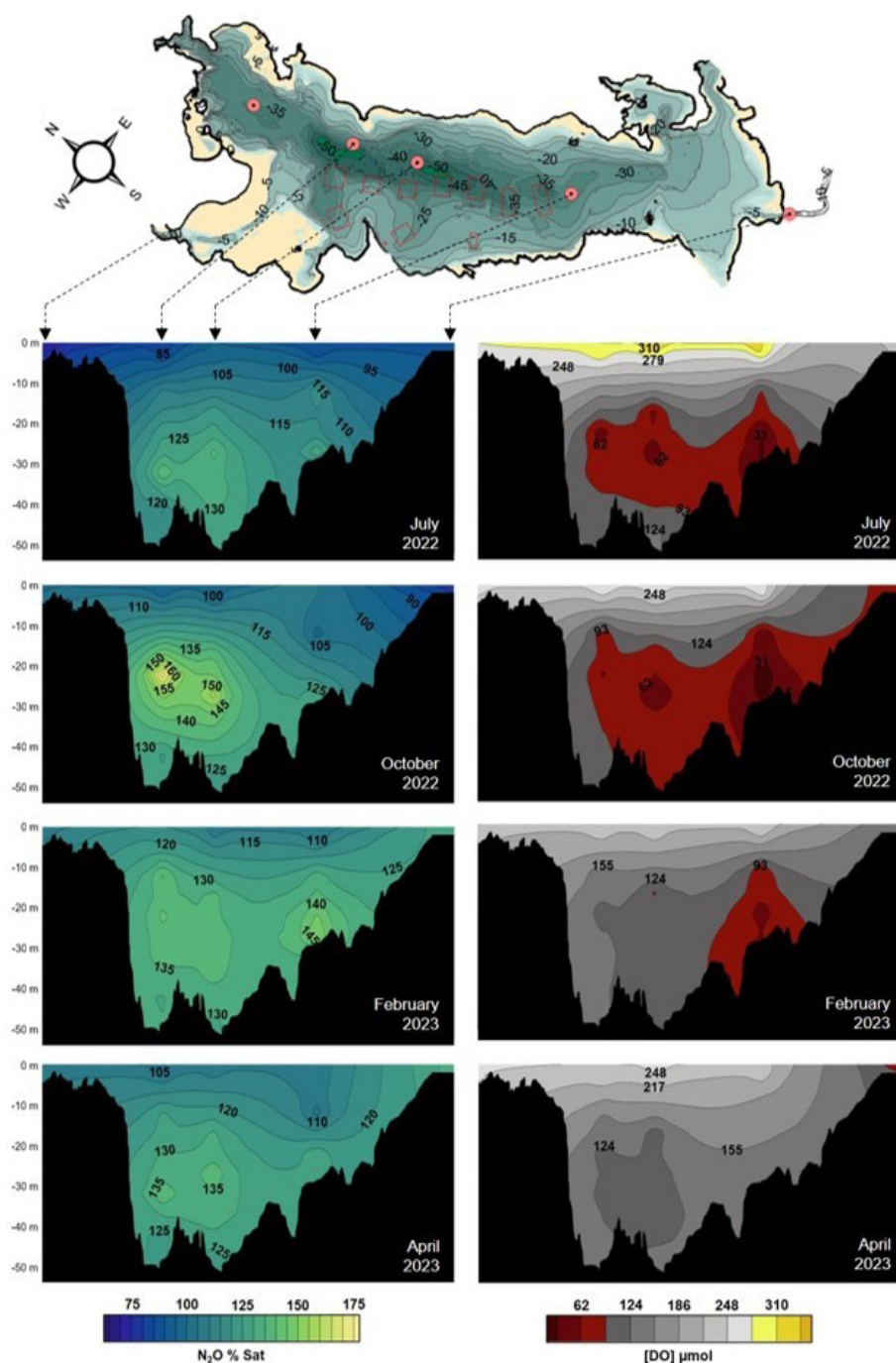
Figure 6. Contour plots of mean N$_2$O % saturation (left column) and mean DO concentration in units of µmol (right column) observed at stations HG3, C10, C08, WH2, and GR1 from July 2022 to April 2023. Shaded red areas on the DO plots indicate low oxygen concentrations (< 93 µmol). Relative positions of the stations are shown in the top-left plot. The y axis displays depth in metres relative to mean sea level.

Bay, southwestern Baltic Sea), indicate a tight coupling between DO supply and N$_2$O production (presumably by nitrification) and consumption (presumably by denitrification) pathways in that area (Ma et al., 2019). The reintroduction of marine water on the upstream side of a dam in the Nakong River, South Korea, was found to affect bottom water trap-

ping (stagnation), DO conditions, N process rates, process-specific gene abundances, and subsequently the fate of N in that system (Huang et al., 2024). Marine intrusions primarily refresh the DO supply adjacent to the sill in Macquarie Harbour (near station C10). As we observed a positive correlation between AOU and ΔN$_2$O marine intrusions offer a
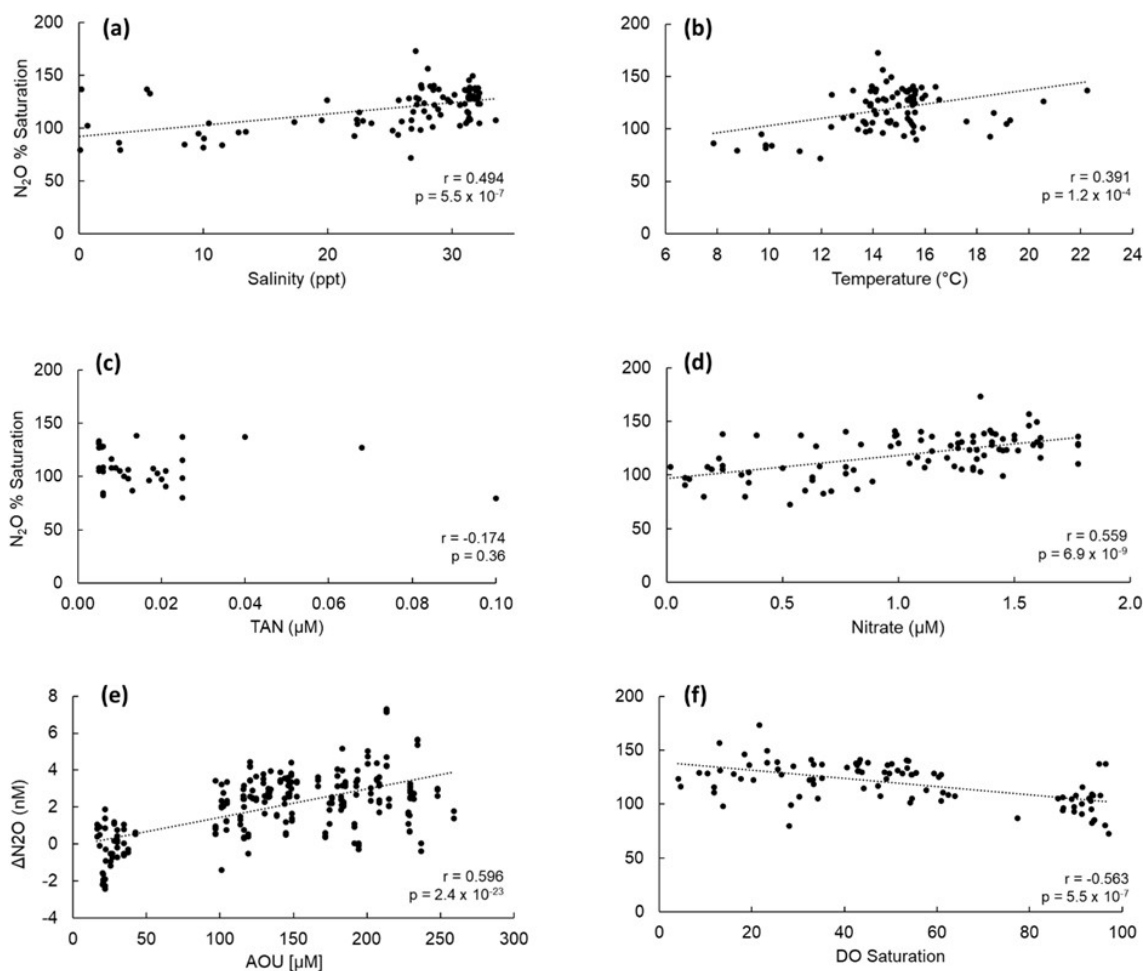
Figure 7. Correlation between N$_2$O percentage saturation observed across the harbour and **(a)** salinity, **(b)** temperature, **(c)** Total Ammoniacal Nitrogen (TAN) concentration, and **(d)** nitrate concentration. The correlation between AOU (µM) and ΔN$_2$O (nM) is shown in **(e)**. The relationship between N$_2$O % saturation and DO % saturation is shown in **(f)**. Pearson correlation coefficients (r) and their associated p values are shown in each panel.

possible explanation for the higher sub-halocline N$_2$O concentrations observed in this part of the harbour (see Fig. 7e).

One other possible pathway of water column N$_2$O production might be through denitrification as DO concentrations at WH2 in October 2022 approached single digits (3.1 µM). This station has the highest basin residence time compared the others used in this study. Low oxygen concentrations may also likely be found under the harbour's fish farms due to the aerobic respiration of farm debris (Maxey et al., 2020). Though whether denitrification functions as a production process or a loss process will depend upon the drivers of DO concentration (i.e. respiration rates, physical mixing, etc.) and may differ depending on the location of the basins in this system. It is likely the main driver of undersaturated N$_2$O concentrations in the Gordon River.

We conceptualise that during periods of high river flow, the surface water lens thickens and transports water undersaturated with N$_2$O quickly across the harbour surface and out of Hells Gates inlet. N$_2$O from the continuously oversaturated sub-halocline water is entrained in the surface lens (diapycnal flux) and transported laterally and out of the system in its dissolved form. During periods of low river flow, the surface lens is thinner and residence times longer (Andrewartha and Wild-Allen, 2017; Maxey et al., 2022). We suspect that N$_2$O from the oversaturated sub-halocline water then diffuses through the surface layer and is emitted into the atmosphere in its gaseous form (Fig. 9). Our estimates of diapycnal flux indicate that the mass transport from sub-halocline waters is smaller ($\sim 2\times$ smaller) than the air–sea flux, supporting this idea. This conceptual model suggests that the harbour surface lens functions to capture both gaseous N$_2$O from the atmosphere and dissolved N$_2$O generated in the sub-halocline layer and transport it to the ocean in its dissolved form during high-flow periods (Fig. 9).

This study focuses on characterising N$_2$O dynamics at end-members and at stations through the harbour's longi-

Table 2. Estimated air–sea N₂O flux (mean µmol N₂O m⁻² d⁻¹ ± SD) of the main harbour stations using calculations presented in Bange et al. (2019) and Zhang et al. (2020) and a range of k_{600} parameterisations from Wanninkhof (2014; W_{2014}), Raymond and Cole (2001; RC_{Low}, RC_{Mid}, and RC_{High}), and Nightingale et al. (2000; N_{2000}). Positive values indicate the flux of N₂O from the harbour water to the atmosphere. Negative values indicate flux of N₂O from the atmosphere into the harbour water. Estimated Gordon River flow and Mean (20 d) Gordon Above Denison (GAD) Stream Gauge data are also shown for each month in addition to the Pearson correlation and associated p values between flow metrics, rainfall, and air–sea flux (and surface water percentage saturation).

Station	K_{600}	Jul 2022 µmol N₂O m⁻² d⁻¹	Oct 2022 µmol N₂O m⁻² d⁻¹	Feb 2023 µmol N₂O m⁻² d⁻¹	Apr 2023 µmol N₂O m⁻² d⁻¹	Gordon flow vs. surface flux	GAD flow vs. surface flux	GAD flow vs. % N₂O sat.	Rainfall vs. surface flux
KR1	RC_{High}:	-11.07 ± 5.17	-04.01 ± 1.77	-03.30 ± 1.54	-03.17 ± 1.66	$r = -0.8316$	$r = -0.8624$	$r = -0.8726$	$r = 0.5577$
	RC_{Mid}:	-08.45 ± 4.42	-03.19 ± 1.59	-02.55 ± 1.34	-02.44 ± 1.41	$p = 7.5 \times 10^{-4}$	$p = 3.1 \times 10^{-4}$	$p = 2.1 \times 10^{-4}$	$p = 0.060$
	RC_{Low}:	-04.69 ± 3.17	-01.93 ± 1.27	-01.46 ± 0.99	-01.38 ± 0.99				
	N_{2000}:	-0.85 ± 0.31	-0.30 ± 0.08	-0.25 ± 0.09	-0.24 ± 0.11				
	W_{2014}:	-0.78 ± 0.25	-0.27 ± 0.05	-0.23 ± 0.07	-0.22 ± 0.09				
C10	RC_{High}:	-12.88 ± 6.00	-01.21 ± 0.53	07.31 ± 3.43	02.60 ± 1.36	$r = -0.8298$	$r = -0.9091$	$r = -0.8795$	$r = 0.2751$
	RC_{Mid}:	-09.83 ± 5.14	-00.96 ± 0.48	05.65 ± 2.98	02.00 ± 1.16	$p = 8.4 \times 10^{-4}$	$p = 4.2 \times 10^{-5}$	$p = 1.6 \times 10^{-4}$	$p = 0.387$
	RC_{Low}:	-05.46 ± 3.68	-00.58 ± 0.38	03.22 ± 2.19	01.13 ± 0.81				
	N_{2000}:	-0.99 ± 0.36	-0.09 ± 0.02	0.67 ± 0.23	0.20 ± 0.09				
	W_{2014}:	-0.91 ± 0.29	-0.08 ± 0.02	0.61 ± 0.18	0.18 ± 0.07				
C08	RC_{High}:	-03.50 ± 1.63	-01.69 ± 0.74	04.08 ± 1.91	04.57 ± 2.40	$r = -0.8547$	$r = -0.8804$	$r = -0.8447$	$r = 0.1846$
	RC_{Mid}:	-02.67 ± 1.40	-01.34 ± 0.67	03.15 ± 1.66	03.52 ± 2.03	$p = 3.97 \times 10^{-4}$	$p = 1.6 \times 10^{-4}$	$p = 5.4 \times 10^{-4}$	$p = 0.566$
	RC_{Low}:	-01.49 ± 1.00	-0.81 ± 0.53	01.80 ± 1.22	01.98 ± 1.43				
	N_{2000}:	-0.27 ± 0.10	-0.12 ± 0.03	0.31 ± 0.10	0.35 ± 0.15				
	W_{2014}:	-0.25 ± 0.08	-0.11 ± 0.02	0.29 ± 0.08	0.32 ± 0.13				
WH2	RC_{High}:	-10.88 ± 5.06	02.63 ± 1.15	02.40 ± 1.13	03.50 ± 1.84	$r = -0.8071$	$r = -0.8269$	$r = -0.8077$	$r = 0.6316$
	RC_{Mid}:	-08.30 ± 4.34	02.09 ± 1.04	01.85 ± 0.98	02.69 ± 1.56	$p = 1.51 \times 10^{-3}$	$p = 9.1 \times 10^{-4}$	$p = 1.5 \times 10^{-3}$	$p = 0.028$
	RC_{Low}:	-04.61 ± 3.11	01.26 ± 0.83	01.06 ± 0.72	01.52 ± 1.09				
	N_{2000}:	-0.84 ± 0.30	0.19 ± 0.05	0.19 ± 0.06	0.27 ± 0.12				
	W_{2014}:	-0.77 ± 0.24	0.17 ± 0.03	0.17 ± 0.05	0.25 ± 0.10				
Gordon River flow (m³ s⁻¹)		383.6 ± 38.9	360.3 ± 54.1	342.6 ± 74.6	324.3 ± 26.6	–	–	–	–
GAD flow (m³ s⁻¹)		107.6 ± 15.9	73.7 ± 12.1	38.8 ± 5.1	30.5 ± 2.2	–	–	–	–

Table 3. Estimated diapycnal N₂O flux (nmol N₂O m⁻² d⁻¹ ± SD) calculated form local buoyancy frequencies from 20 to 2 m within the main harbour stations. Positive values indicate the flux of N₂O from the basin water (20 m) to the surface lens (2 m).

Station	July 2022 nmol N₂O m⁻² d⁻¹	October 2022 nmol N₂O m⁻² d⁻¹	February 2023 nmol N₂O m⁻² d⁻¹	April 2023 nmol N₂O m⁻² d⁻¹
KR1	80 ± 3.5	282 ± 17.7	992 ± 12.9	395 ± 8.6
C10	140 ± 4.5	1200 ± 47.3	1040 ± 65.3	454 ± 16.2
C08	49 ± 2.3	782 ± 12.1	778 ± 37.4	348 ± 18.6
WH2	117 ± 4.0	125 ± 2.8	$1,308 \pm 67.8$	240 ± 18.0

tudinal axis. Other areas of the harbour, most prominently the shallow embayments around the parameter of the system and the areas occupied by fin fish farms, were not included here. Fin fish aquaculture can increase water column DO demand near the pens in this system (Maxey et al., 2020) and introduces particulate organic material to the water. Whether this manifests in altered N cycling dynamics (especially DO-sensitive processes like nitrification and denitrification) would be system specific and has never been described in this system. High particle loads have been shown to induce denitrification in normoxic waters (e.g. Wan et al., 2023; Frey et al., 2020; Codispoti et al., 2005; Nevison

et al., 2003; Usui et al., 2001; Robinson et al., 1998), and thus an N₂O sink might be present even under farms even in more oxygenated basins. Future studies should investigate the impacts of fin fish aquaculture on DO and N₂O cycling.

One source of uncertainty in our approach is in using literature-derived estimators for air–sea and diapycnal flux estimations. We also used literature-derived k_{600} estimates from Nightingale et al. (2000), Raymond and Cole (2001), and Wanninkhof (2014) to compute N₂O air–sea flux. Literature-derived estimators of K_{600} and eddy diffusivity are commonly used when direct measurements are unavailable (Tang et al., 2024; Li et al., 2023; Murray et al.,
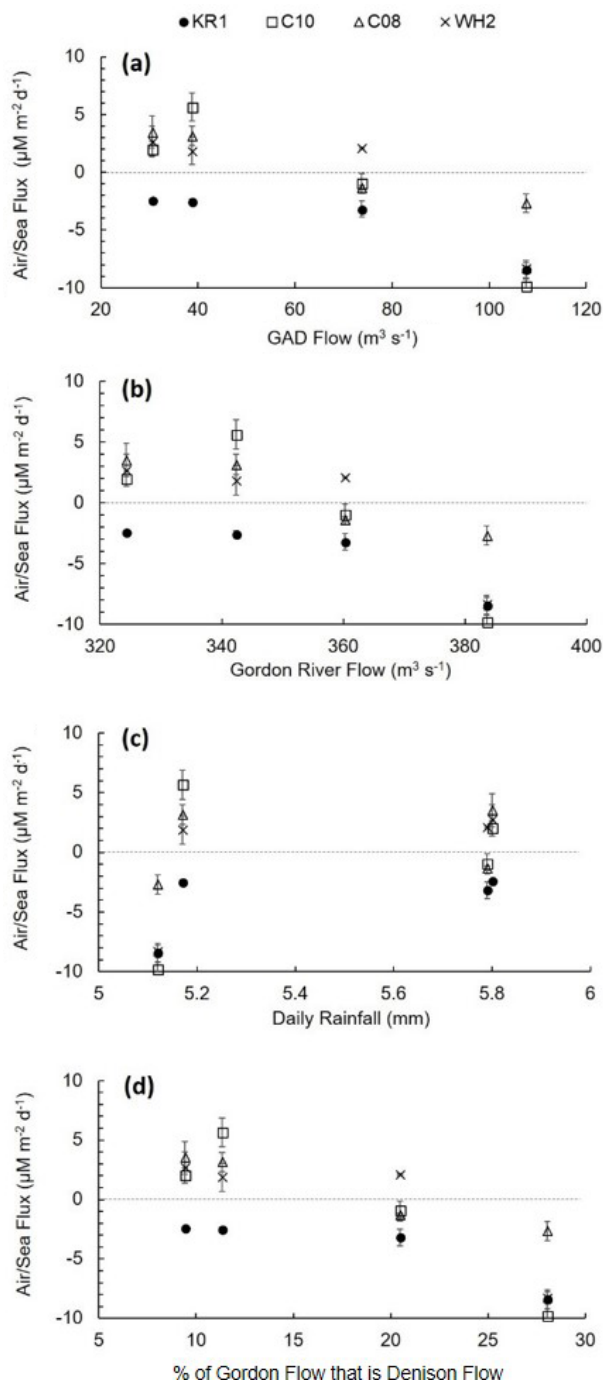
Figure 8. Mean air–sea flux ($\mu M\,m^{-2}\,d^{-1}$) vs. **(a)** GAD flow ($m^3\,d^{-1}$), **(b)** estimated Gordon River flow ($m^3\,d^{-1}$), **(c)** daily rainfall (mm) (20 d mean), and **(d)** percentage of estimated Gordon River flow. These variables are accounted for by the GAD Stream Gauge (proxy for hydroelectric dam release)Ėrror bars indicate ± 1 standard error.

2020), but to reduce uncertainty these are ideally measured in situ. Likewise, we presented diapycnal flux estimates using turbulent eddy diffusivities from Fer (2006) that were not measured in Macquarie Harbour.

Previous work in Australian estuaries with pristine catchments (like Macquarie Harbour) has shown that many tend to function as a sink for atmospheric N_2O (Maher et al., 2016; Wells et al., 2018). Our study adds the caveat that water column and atmospheric exchange may also depend on factors controlling river flow in deeper stratified systems. Despite the advancements made to date, many of the deeper estuaries in Chile, Australia, and New Zealand are lacking descriptions of N_2O exchange between the water column and atmosphere (e.g. Bathurst Harbour, Tasmania; fjords of the South Island, New Zealand; estuaries on Stewart Island, New Zealand). Given that these systems have relatively pristine catchments, they offer an opportunity to better understand natural fjord-like estuarine responses to the climate drivers of N_2O dynamics. Mesoscale climate oscillations (i.e. the SAM and NAO) have been shown to affect rainfall, river flow, and DO concentrations in this and other fjord-like estuaries (Maxey et al., 2022; Austin and Inall, 2002). In western Tasmania, SAM in its positive phase results in increased orographic rainfall and a greater propensity for higher river flow, possibly tilting the source and sink balance to net N_2O uptake during these periods.

Climate change predictions for Tasmania's western Coast (which includes the Macquarie Harbour catchment) indicate that the region will experience a more extreme precipitation regime with increased winter precipitation and decreased summer precipitation (Grose et al., 2010; Bennett et al., 2010). If these future predictions result in more extreme seasonality in Gordon River flow, then the harbour may respond in kind with a larger variation in N_2O air–sea flux, i.e. greater N_2O atmospheric uptake in winter and greater N_2O emission in summer. However, given that the river flow is somewhat regulated by the hydroelectric dam, our study suggests that flow regulation has the potential to augment harbour N_2O emissions. Releasing water during extreme low-rainfall periods might allow N_2O slowly accumulating in sub-halocline waters to be released in the exported surface lens. Fjords and fjord-like estuaries are defined by their strong stratification and sensitivity to freshwater inputs. With climate change, rainfall patterns are expected to become more extreme and thus alter the river flow and subsequently N_2O source sink dynamics in these systems on a global scale. In systems that are expected to experience increasingly drier conditions, they may shift from net sinks of N_2O to sources and further perpetuate the accumulation of N_2O in the atmosphere.

It is well established that fjord and fjord-like estuaries are important sites of C burial (Smith et al., 2015; Bianchi et al., 2018, 2020). This study supports the idea that they can also be important sites of atmospheric N_2O removal and transport. Macquarie Harbour air–sea flux estimates are similar in magnitude to observations made in other stratified estuar-
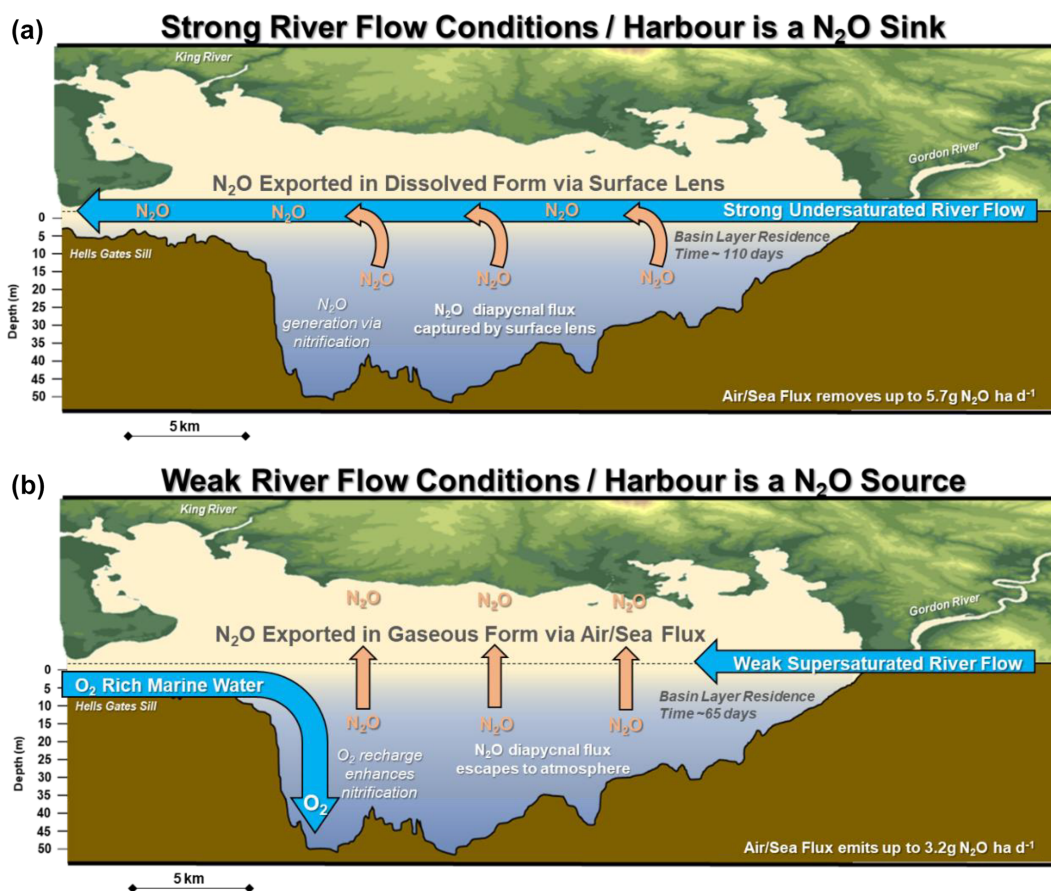
Figure 9. Conceptual model of Macquarie Harbour's N$_2$O dynamics. Panel (**a**) depicts the capture of N$_2$O generated in the sub-halocline during strong river flow conditions. Here N$_2$O is exported from the harbour in its dissolved form via undersaturated surface flows from the harbour to the ocean. Panel (**b**) depicts the efflux of N$_2$O from the harbour surface during low-flow conditions. Note that during these conditions the surface flows are weak and generally supersaturated with N$_2$O, permitting its escape in gaseous form to the atmosphere.

ies and enclosed seas such as the Reloncaví Estuary, Chile (Yevenes et al., 2017), and Eckernförde Bay, Germany (Ma et al., 2019) (Table A1). Macquarie Harbour, however, was observed to have lower fluxes of N$_2$O into the atmosphere than other river-dominated (but not fjord-like) estuaries (Elbe River, Germany; Schulz et al., 2023) including those on the Australian mainland's east coast (Wells et al., 2018).

tion indicates that the main N$_2$O generation process is likely nitrification. Climate change is predicted to result in wetter winters and drier summers for the western coast of Tasmania, which may result in augmented N$_2$O air–sea fluxes. This work represents the first descriptions of N$_2$O spatiotemporal distribution, estimated air–sea flux, estimated diapycnal flux, and N$_2$O production pathways in this system.

5   Conclusions

In summary, river flow, and specifically river flow driven by hydroelectric dam release, significantly affects both surface water N$_2$O concentrations and air–sea flux in Macquarie Harbour. Importantly, when river flow is low, most of the harbour emits N$_2$O to the atmosphere. When river flow is high, most of the harbour removes N$_2$O from the atmosphere, intercepts the diapycnal flux, and laterally exports this N$_2$O to the ocean in its dissolved form. N$_2$O is continually supersaturated below the halocline, and the relationship between AOU and ΔN$_2$O and N$_2$O saturation and NO$_3^-$ concentra-

Appendix A

Table A1. N_2O fluxes and observed ranges of mean ($\pm$ SD) N_2O concentration and saturation from both fjord-like and river-dominated estuaries around the globe and estuaries in Australia.

Location	System type	Measurement depth range	Mean air–sea N_2O flux (μMol $N_2O\,m^{-2}\,d^{-1}$)	Min and max air–sea N_2O flux (μMol $N_2O\,m^{-2}\,d^{-1}$)	Mean N_2O concentration (saturation) nM N_2O (%)	Min and max N_2O concentration (saturation) nM N_2O (%)	Reference
Macquarie Harbour, western Tasmania, Australia	Fjord-like estuary	2 to 45 m	-09.83 ± 0.67 to 05.65 ± 1.22	-10.82 to 7.73	11.7 ± 1.6 (121.8 $\pm$ 17.8)	7.87 to 17.12 (81 to 174)	This study
Reloncaví Estuary, Chile	Fjord-like estuary	0 to 5 m	0.86 ± 2.28	-1.58 to 5.60	11.8 ± 1.70 (111 $\pm$ 18.3)	8.34 to 14.5 (80 to 140)	Yevenes et al. (2017)
Reloncaví Estuary, Chile	Fjord-like estuary	10 to 200 m	–	–	14.5 ± 1.73 (145 $\pm$ 17.7)	10.5 to 17.0 (11 to 170)	Yevenes et al. (2017)
Chiloé Interior Sea, Chile	Fjord-like estuary	0 to 200 m	1.08 ± 1.41	-0.18 to 3.19	12.6 ± 2.36 (121 $\pm$ 17.5)	8.81 to 21.1 (87 to 160)	Yevenes et al. (2017)
Europa Sound, Magallanes Region, Chile	Fjord-like estuary	1 to 10 m	-15.22 to -0.81	–	11.9 ± 5.7 to 12.7 ± 1.0	–	Farías et al. (2018)
Concepción Channel, Magallanes Region, Chile	Fjord-like estuary	1 to 150 m	0.69 to 7.70	–	13.6 ± 1.1 to 17.0 ± 0.02	-	Farías et al. (2018)
Sarmiento Channel, Magallanes Region, Chile	Fjord-like estuary	1 to 10 m	2.07 to 12.53	–	13.1 ± 0.1 to 16.5 ± 0.3	-	Farías et al. (2018)
Estero Peel, Magallanes Region, Chile	Fjord-like estuary	1 to 10 m	0.11 to 2.01	–	13.1 ± 0.2 to 13.5 ± 0.5	–	Farías et al. (2018)
Estero Calvo, Magallanes Region, Chile	Fjord-like estuary	1 to 10 m	0.04	–	13.9 ± 0.8	–	Farías et al. (2018)
Estero Amalia, Magallanes Region, Chile	Fjord-like estuary	1 to 100 m	-0.08	–	14.2 ± 1.7	–	Farías et al. (2018)
Estero las Montañas, Magallanes Region, Chile	Fjord-like estuary	1 to 10 m	-2.95	–	9.69 ± 1.6	–	Farías et al. (2018)
Smyth Channel, Magallanes Region, Chile	Fjord-like estuary	1 to 300 m	1.07 to 11.2	–	14.3 ± 0.4 to 16.0 ± 0.5	-	Farías et al. (2018)
Última Esperanza Sound, Magallanes Region, Chile	Fjord-like estuary	1 to 10 m	-3.7 to 10.4	–	12.1 ± 1.1 to 13.7 ± 0.07	–	Farías et al. (2018)
Almirante Montt Gulf, Magallanes Region, Chile	Fjord-like estuary	1 to 150 m	15.6	–	21.0 ± 5.7	–	Farías et al. (2018)
Kirke Channel, Magallanes Region, Chile	Fjord-like estuary	1 to 10 m	0.12 to 8.19	–	13.3 ± 0.1 to 15.4 ± 0.4	–	Farías et al. (2018)
Union Channel, Magallanes Region, Chile	Fjord-like estuary	1 to 10 m	22.1	–	16.7 ± 0.8	–	Farías et al. (2018)

Table A1. Continued.

Location	System type	Measurement depth range	Mean air–sea N$_2$O flux (μMol N$_2$O m^{-2} d^{-1})	Min and max air–sea N$_2$O flux (μMol N$_2$O m^{-2} d^{-1})	Mean N$_2$O concentration (saturation) nM N$_2$O (%)	Min and max N$_2$O concentration (saturation) nM N$_2$O (%)	Reference
Union Sound, Magallanes Region, Chile	Fjord-like estuary	1 to 10 m	2.86	–	14.8 ± 0.8	–	Farías et al. (2018)
Western Strait of Magellan, Magallanes Region, Chile	Fjord-like Estuary	1 to 10 m	143	–	15.71	–	Farías et al. (2018)
Eastern Strait of Magellan, Magallanes Region, Chile	Fjord-like estuary	1 m	36.3	–	16.4	–	Farías et al. (2018)
San Gregorio Cape, Magallanes Region, Chile	Fjord-like estuary	1 m	24.8	–	12.07	–	Farías et al. (2018)
Central Otway Sound, Magallanes Region, Chile	Fjord-like estuary	1 m	35.5	–	11.4	–	Farías et al. (2018)
Northern Magdalena Channel, Magallanes Region, Chile	Fjord-like estuary	1 m	−0.22	–	11.4	–	Farías et al. (2018)
Chasco Sound, Magallanes Region, Chile	Fjord-like estuary	1 m	6.81	–	16.01	–	Farías et al. (2018)
Western Cockburn Channel, Magallanes Region, Chile	Fjord-like estuary	1 m	6.18	–	14.47	–	Farías et al. (2018)
Saanich Inlet, British Columbia, Canada	Fjord-like estuary	10 to 200 m	2.3 ± 2.5 to 3.9 ± 2.9	–	14.7	< 0.5 to 37.4	Capelle et al. (2018)
Saanich Inlet, British Columbia, Canada	Fjord-like estuary	Surface to 110 m	11.3 to 20.4	–	–	–	Cohen (1978)
Elbe River estuary, Germany	Well-mixed river-dominated estuary	1.2 m	–	26.0 ± 23.5 to 100.7 ± 101.2	–	(161 ± 53.6) to (243 ± 141.6)	Schulz et al. (2023)
Eckernförde Bay, Boknis Eck Time Series Station, Baltic Sea, Germany	Enclosed sea	1 to 25 m	3.5 ± 12.4	−19.0 to 105.7	(111 ± 30)	(56 to 314)	Ma et al. (2019)
Eckernförde Bay, Boknis Eck Time Series Station, Baltic Sea, Germany	Enclosed sea	1 to 25 m	–	–	10 to 17	–	Walter et al. (2006)

Table A1. Continued.

Location	System type	Measurement depth range	Mean air–sea N_2O flux (μMol $N_2O\,m^{-2}\,d^{-1}$)	Min and max air–sea N_2O flux (μMol $N_2O\,m^{-2}\,d^{-1}$)	Mean N_2O concentration (saturation) nM N_2O (%)	Min and max N_2O concentration (saturation) nM N_2O (%)	Reference
Baltic Sea, Germany	Enclosed sea	110 m	5–11	–	14 to 1523	–	Rönner (1983)
Gotland Basin, Baltic Sea, Germany	Enclosed sea	90 m	–	–	13	0 to 126 (0 to 450)	Brettar and Rheinheimer (1991)
Northwestern Shelf, Black Sea	Enclosed sea	–	1.6 to 4.4	–	6.5 to 8	–	Amouroux et al. (2002)
Northwestern Black Sea Shelf, Black Sea	Enclosed sea	70 m	3.1 to 5.2	–	7.5 to 10.2	–	Amouroux et al. (2002)
Cariaco Basin, Venezuela	Coastal basin	Surface to 400 m	–	–	4.4 to 5.5	–	Hashimoto et al. (1983)
Guadalquivir Estuary, Gulf of Cádiz, Spain	River-dominated estuary	2 m	18.7 ± 33.6	–	20.6 ± 24.3	–	Sierra et al. (2020)
Guadalquivir Estuary, Gulf of Cádiz, Spain	River-dominated estuary	2 m	0.3 ± 0.5	–	6.7 ± 0.4	–	Sierra et al. (2020)
Guadalquivir Estuary, Gulf of Cádiz, Spain	River-dominated estuary	2 m	0.9 ± 21.6	–	7.3 ± 15.4	–	Sierra et al. (2020)
Noosa River estuary, eastern Australia	River-dominated estuary	0.5 to 9.6 m	-14.24 ± 14.02	$-57.72\,to\,22.20$	6.99 ± 0.43 (97 ± 2.2)	5.92 to 7.95 (90 to 103)	Wells et al. (2018)
Mooloolah River estuary, eastern Australia	River-dominated estuary	0.5 to 6.8 m	-7.33 ± 7.25	$-48.76\,to\,16.31$	6.74 ± 0.64 (97 ± 3.8)	5.19 to 7.71 (82 to 112)	Wells et al. (2018)
Maroochy River estuary, eastern Australia	River-dominated estuary	0.5 to 8.2 m	51.33 ± 55.3	-34.94 to 179.64	8.4 ± 1.50 (113 ± 16.7)	6.07 to 12.93 (92 to 163)	Wells et al. (2018)
Pine River estuary, eastern Australia	River-dominated estuary	0.5 to 10.1 m	17.10 ± 39.44	-33.22 to 145.50	7.1 ± 0.76 (102 ± 6.24)	6.05 to 8.57 (93 to 117)	Wells et al. (2018)
Brisbane River estuary, eastern Australia	River-dominated estuary	0.5 to 23.9 m	209.54 ± 143.59	15.42 to 662.62	9.8 ± 1.36 (133 ± 9.9)	6.75 to 12.75 (105 to 158)	Wells et al. (2018)
Middle reach, Brisbane River estuary, eastern Australia	River-dominated estuary	Surface	14.5 ± 1.19	5.4 ± 0.34 to 25.2 ± 1.87	–	13.1 to 17.9 (160 to 250)	Sturm et al. (2017)
Lower reach, Brisbane River estuary, eastern Australia	River-dominated estuary	Surface	$6. \pm 0.51$	3.7 ± 0.85 to 9.1 ± 1.19	–	9.2 to 12.7 (125 to 410)	Sturm et al. (2017)
Oxley Creek, eastern Australia	River-dominated estuary	2.1 to 13.1 m	210.59 ± 60.23	$91.54\,to\,280.16$	11.7 ± 1.34 (156 ± 19.7)	9.65 to 14.89 (139 to 199.7)	Wells et al. (2018)

Table A1. Continued.

Location	System type	Measurement depth range	Mean air–sea N$_2$O flux (µMol N$_2$O m^{-2} d^{-1})	Min and max air–sea N$_2$O flux (µMol N$_2$O m^{-2} d^{-1})	Mean N$_2$O concentration (saturation) nM N$_2$O (%)	Min and max N$_2$O concentration (saturation) nM N$_2$O (%)	Reference
Nerang River estuary, eastern Australia	River-dominated estuary	0.5 to 6.8 m	-0.62 ± 20.87	-67.98 to 45.92	6.73 ± 0.43 (100 ± 4.3)	5.99 to 7.79 (88 to 109)	Wells et al. (2018)
Logan River estuary, eastern Australia	–	0.5 to 14.4 m	110.00 ± 153.55	-54.48 to 796.00	9.3 ± 2.36 (127 ± 27.5)	5.54 to 14.8 (81 to 191)	Wells et al. (2018)
Albert River estuary, eastern Australia	–	1.1 to 15.7 m	90.05 ± 73.32	-9.50 to 264.25	10.10 ± 2.24 (131 ± 29.8)	7.32 to 15.1 (98 to 205)	Wells et al. (2018)
Darwin Creek, Australia	Mangrove creek	∼ 1 m	-0.12	–	6.3 (98.9)	6.0 to 6.8 (95 to 104)	Maher et al. (2016)
Hinchinbrook Creek, Australia	Mangrove creek	∼ 1 m	-3.43	–	6.1 (83.3)	5.6 to 6.8 (75 to 91)	Maher et al. (2016)
Melbourne Creek, Australia	Mangrove creek	∼ 1 m	-1.33	–	7.9 (96.6)	6.9 to 9.1 (86 to 115)	Maher et al. (2016)
Morton Bay Creek, Australia	Mangrove creek	∼ 1 m	-3.19	–	5.1 (77.4)	3.4 to 6.6 (50 to 105)	Maher et al. (2016)
Seventeen Seventy Creek, Australia	Mangrove creek	∼ 1 m	-1.75	–	7.7 (94.3)	7.1 to 8.9 (88 to 106)	Maher et al. (2016)
Brisbane River, Australia	–	–	–	–	(285)	(135 to 435)	Musenze et al. (2014)
Coffs Creek, Australia	–	–	–	–	(219 ± 37)	(53 to 386)	Reading et al. (2017)
Coffs Creek, Australia	–	–	–	–	(266.5 ± 128)	(86 to 678)	Reading et al. (2020)
Boambee Creek, Australia	–	–	–	–	(197.1 ± 75)	(87 to 329)	Reading et al. (2020)
Bonville Creek, Australia	–	–	–	–	(183.7 ± 65)	(78 to 310)	Reading et al. (2020)
Pine Creek, Australia	–	–	-	–	(194.1 ± 65)	(79 to 382)	Reading et al. (2020)
Yarra River, Australia	Salt wedge estuary	–	–	–	(135.9 ± 31)	–	Tait et al. (2017)

References

Abril, G. and Borges, A. V.: Carbon Dioxide and Methane Emissions from Estuaries, in: Greenhouse Gas Emissions-Fluxes and Processes: Hydroelectric Reservoirs and Natural Environments, 187–207, Berlin, Heidelberg: Springer Berlin Heidelberg, https://doi.org/10.1007/978-3-540-26643-3_8, 2004.

Acuña-González, J. A., Vargas-Zamora, J. A., and Córdoba-Muñoz, R.: A snapshot view of some vertical distributions of water parameters at a deep (200 m) station in the fjord-like Golfo Dulce, embayment, Costa Rica, Rev. Biol. Trop., 54, 193–200, ISSN: 0034-7744, 2006.

Amouroux, D., Roberts, G., Rapsomanikis, S., and Andreae, M. O.: Biogenic gas (CH_4, N_2O, DMS) emission to the atmosphere from near-shore and shelf waters of the north-western Black Sea, Estuar. Coast. Shelf Sci., 54, 575–587, https://doi.org/10.1006/ecss.2000.0666, 2002.

Andrewartha, J. and Wild-Allen, K.: CSIRO Macquarie Harbour Hydrodynamic and Oxygen Tracer Modelling, Progress report to FRDC 2016/067 Project Steering Committee, 2017.

Arneborg, L., Janzen, C., Liljebladh, B., Rippeth, T. P., Simpson, J. H., and Stigebrandt, A.: Spatial variability of diapycnal mixing and turbulent dissipation rates in a stagnant fjord basin, J. Phys. Oceanogr., 34, 1679–1691, https://doi.org/10.1175/1520-0485(2004)034<1679:SVODMA>2.0.CO;2, 2004.

Austin, W. E. and Inall, M. E.: Deep-water renewal in a Scottish fjord: temperature, salinity and oxygen isotopes, Polar Res., 21, 251–257, https://doi.org/10.3402/polar.v21i2.6485, 2002.

Bange, H. W.: Nitrous oxide and methane in European coastal waters, Estuarine, Coast. Shelf Sci., 70, 361–374, https://doi.org/10.1016/j.ecss.2006.05.042, 2006.

Bange, H. W., Rapsomanikis, S., and Andreae, M. O.: Nitrous oxide in coastal waters, Global Biogeochem. Cy., 10, 197–207, https://doi.org/10.1029/95GB03834, 1996.

Bange, H. W., Bell, T. G., Cornejo, M., Freing, A., Uher, G., Upstill-Goddard, R. C., and Zhang, G. L.: MEMENTO: A proposal to develop a database of marine nitrous oxide and methane measurements, Environ. Chem., 6, 195–197, https://doi.org/10.1071/en09033, 2009 (data available at: https://memento.geomar.de, last access: 9 December 2024).

Bange, H. W., Sim, C. H., Bastian, D., Kallert, J., Kock, A., Mujahid, A., and Müller, M.: Nitrous oxide (N_2O) and methane (CH_4) in rivers and estuaries of northwestern Borneo, Biogeosciences, 16, 4321–4335, https://doi.org/10.5194/bg-16-4321-2019, 2019.

Bange, H. W., Mongwe, P., Shutler, J. D., Arévalo-Martínez, D. L., Bianchi, D., Lauvset, S. K., Liu, C., Löscher, C. R., Martins, H., Rosentreter, J. A., Schmale, O., Steinhoff, T., Upstill-Goddard, R. C., Wanninkhof, R., Wilson, S. T., and Xie, H.: Advances in understanding of air–sea exchange and cycling of greenhouse gases in the upper ocean, Elementa: Science of the Anthropocene, 12, 1, https://doi.org/10.1525/elementa.2023.00044, 2024.

Bastian, D.: N_2O und CH_4 Verteilung in Ästuaren und Flüssen im Nordwesten von Borneo, BSc thesis, Kiel University, Kiel, 50 pp., 2017.

Baulch, H. M., Schiff, S. L., Maranger, R., and Dillon, P. J.: Nitrogen enrichment and the emission of nitrous oxide from streams, Global Biogeochem. Cy., 25, GB4013, https://doi.org/10.1029/2011GB004047, 2011.

Beaulieu, J. J., Shuster, W. D., and Rebholz, J. A.: Controls on gas transfer velocities in a large river, J. Geophys. Res.-Biogeo., 117, G02007, https://doi.org/10.1029/2011JG001794, 2012.

Bennett, J. C., Ling, F. L. N., Graham, B., Grose, M. R., Corney, S. P., White, C. J., Holz, G. K., Post, D. A., Gaynor, S. M. and Bindoff, N. L.: Climate Futures for Tasmania: water and catchments technical report, Antarctic Climate & Ecosystems Cooperative Research Centre, Hobart, Tasmania, ISBN 978-1-921197-06-8, 2010.

Bianchi, T. S., Cui, X., Blair, N. E., Burdige, D. J., Eglinton, T. I., and Galy, V.: Centers of organic carbon burial and oxidation at the land-ocean interface, Org. Geochem., 115, 138–155, https://doi.org/10.1016/j.orggeochem.2017.09.008, 2018.

Bianchi, T. S., Arndt, S., Austin, W. E., Benn, D. I., Bertrand, S., Cui, X., Faust, J., Koziorowska-Makuch, K., Moy, C., Savage, C., Smeaton, C., Smith, R., and Syvitski, J.: Fjords as aquatic critical zones (ACZs), Earth-Sci. Rev., 203, 103145, https://doi.org/10.1016/j.earscirev.2020.103145, 2020.

Brase, L., Bange, H. W., Lendt, R., Sanders, T., and Dähnke, K.: High resolution measurements of nitrous oxide (N₂O) in the Elbe estuary, Front. Mar. Sci., 4, 162, https://doi.org/10.3389/fmars.2017.00162, 2017.

Breider, F., Yoshikawa, C., Makabe, A., Toyoda, S., Wakita, M., Matsui, Y., Kawagucci, S., Fujiki, T., Harada, N., and Yoshida, N.: Response of N₂O production rate to ocean acidification in the western North Pacific, Nat. Clim. Change, 9, 954–958, https://doi.org/10.1038/s41558-019-0605-7, 2019.

Brettar, I. and Rheinheimer, G.: Denitrification in the Central Baltic: evidence for H₂S-oxidation as motor of denitrification at the oxic-anoxic interface, Mar. Ecol. Prog. Ser., 77, 157–169, http://www.jstor.org/stable/24826569, 1991.

Bourbonnais, A., Lehmann, M. F., Hamme, R. C., Manning, C. C., and Juniper, S. K.: Nitrate elimination and regeneration as evidenced by dissolved inorganic nitrogen isotopes in Saanich Inlet, a seasonally anoxic fjord, Mar. Chem., 157, 194–207, https://doi.org/10.1016/j.marchem.2013.09.006, 2013.

Capelle, D. W., Hawley, A. K., Hallam, S. J., and Tortell, P. D.: A multi-year time-series of N₂O dynamics in a seasonally anoxic fjord: Saanich Inlet, British Columbia, Limnol. Oceanogr., 63, 524–539, https://doi.org/10.1002/lno.10645, 2018.

Carpenter, P. D., Butler, E. C. V., Higgins, H. W., Mackey, D. J., and Nichols, P. D.: Chemistry of trace elements, humic substances and sedimentary organic matter in Macquarie Harbour, Tasmania, Mar. Freshwater Res., 42, 625–654, https://doi.org/10.1071/MF9910625, 1991.

Chen, C., Pan, J., Xiao, S., Wang, J., Gong, X., Yin, G., Hou, L., Liu, M., and Zheng, Y.: Microplastics alter nitrous oxide production and pathways through affecting microbiome in estuarine sediments, Water Res., 221, 118733, https://doi.org/10.1016/j.watres.2022.118733, 2022.

Chen, J., Wells, N. S., Erler, D. V., and Eyre, B. D.: Land-use intensity increases benthic N₂O emissions across three sub-tropical estuaries, J. Geophys. Res.-Biogeo., 127, e2022JG006899, https://doi.org/10.1029/2022JG006899, 2022.

Codispoti, L. A., Yoshinari, T., and Devol, A. H.: Suboxic respiration in the oceanic water column, Respiration in Aquatic Ecosystems, 225–247, https://doi.org/10.1093/acprof:oso/9780198527084.001.0001, 2005.

Cohen, Y.: Consumption of dissolved nitrous oxide in an anoxic basin, Saanich Inlet, British Columbia, Nature, 272, 5650, 235–237, https://doi.org/10.1038/272235a0, 1978.

Cresswell, G. R., Edwards, R. J., and Barker, B. A.: Macquarie Harbour, Tasmania-seasonal oceanographic surveys in 1985, University of Tasmania Journal contribution, https://doi.org/10.26749/rstpp.123.63, 1989.

Da Silva, R. R. P., White, C. A., Bowman, J. P., Bodrossy, L., Bissett, A., Revill, A., Eriksen, R., and Ross, D. J.: Network and Machine Learning Analyses of Estuarine Microbial Communities Along a Freshwater-Marine Mixed Gradient, Estuarine, Coast. Shelf Sci., 277, 108026, https://doi.org/10.1016/J.ecss.2022.108026, 2022.

de Bie, M. J. M.: Factors controlling nitrification and nitrous oxide production in the Schelde estuary, Doctoral dissertation, Yerseke, Netherlands Institute of Ecology (NIOO-CEMO), 2002.

Dey, R., Lewis, S. C., Arblaster, J. M., and Abram, N. J.: A review of past and projected changes in Australia's rainfall, Wiley Interdisciplinary Reviews: Climate Change, 10, e577, https://doi.org/10.1002/wcc.577, 2019.

Etminan, M., Myhre, G., Highwood, E. J., and Shine, K. P.: Radiative forcing of carbon dioxide, methane, and nitrous oxide: A significant revision of the methane radiative forcing, Geophys. Res. Lett., 43, 12–614, https://doi.org/10.1002/2016GL071930, 2016.

Eyring, V., Gillett, N. P., Achuta Rao, K. M., Barimalala, R., Barreiro Parrillo, M., Bellouin, N., Cassou, C., Durack, P. J., Kosaka, Y., McGregor, S., Min, S., Morgenstern, O., Sun, Y.: Human Influence on the Climate System, in: Climate Change 2021: The Physical Science Basis, Contribution of Working Group I to the Sixth Assessment Report of the Intergovernmental Panel on Climate Change, edited by: Masson-Delmotte, V., Zhai, P., Pirani, A., Connors, S. L., Péan, C., Berger, S., Caud, N., Chen, Y., Goldfarb, L., Gomis, M. I., Huang, M., Leitzell, K., Lonnoy, E., Matthews, J. B. R., Maycock, T. K., Waterfield, T., Yelekçi, O., Yu, R., and Zhou, B., Cambridge University Press, Cambridge, United Kingdom and New York, NY, USA, 423–552, https://doi.org/10.1017/9781009157896.005, 2021.

Farías, L., Bello, E., Arancibia, G., and Fernandez, J.: Distribution of dissolved methane and nitrous oxide in Chilean coastal systems of the Magellanic Sub-Antarctic region (50° – 55° S), Estuar. Coast. Shelf Sci., 215, 225–240, https://doi.org/10.1016/j.ecss.2018.10.020, 2018.

Fer, I.: Scaling turbulent dissipation in an Arctic fjord, Deep-Sea Res. Pt. II, 53, 77–95, https://doi.org/10.1016/j.dsr2.2006.01.003, 2006.

Forster P., Storelvmo T., Armour K., Collins W., Dufresne J.-L., Frame D., Lunt, D., Mauritsen, T., Palmer, M., Watanabe, M., Wild, M.: The earth's energy budget, climate feedbacks, and climate sensitivity In Climate Change 2021: The Physical Science Basis. Contribution of Working Group I to the Sixth Assessment Report of the Intergovernmental Panel on Climate Change, edited by: Masson-Delmotte, V., Zhai, P., Pirani, A., Connors, S. L., Péan, C., Berger, S., Caud, N., Chen, Y., Goldfarb, L., Gomis, M. I., Huang, M., Leitzell, K., Lonnoy, E., Matthews, J. B. R., Maycock, T. K., Waterfield, T., Yelekçi, O., Yu, R., and Zhou, B., Cambridge University Press, Cambridge, United Kingdom and New York, NY, USA, 423–552, https://doi.org/10.1017/9781009157896.009, 2021.

Frey, C., Bange, H. W., Achterberg, E. P., Jayakumar, A., Löscher, C. R., Arévalo-Martínez, D. L., León-Palmero, E., Sun, M., Sun, X., Xie, R. C., Oleynik, S., and Ward, B. B.: Regulation of nitrous oxide production in low-oxygen waters off the coast of Peru, Biogeosciences, 17, 2263–2287, https://doi.org/10.5194/bg-17-2263-2020, 2020.

Gilbert, D., Rabalais, N. N., Díaz, R. J., and Zhang, J.: Evidence for greater oxygen decline rates in the coastal ocean than in the open ocean, Biogeosciences, 7, 2283–2296, https://doi.org/10.5194/bg-7-2283-2010, 2010.

Gillibrand, P. A., Cage, A. G., and Austin, W. E. N.: A preliminary investigation of basin water response to climate forcing in a Scot-

tish fjord: evaluating the influence of the NAO, Cont. Shelf Res., 25, 571–587, https://doi.org/10.1016/j.csr.2004.10.011, 2005.

Grose, M. R., Barnes-Keoghan, I., Corney S. P., White C. J., Holz, G. K., Bennett, J. B., Gaynor, S. M., and Bindof, N. L.: Climate Futures for Tasmania: general climate impacts technical report, Antarctic Climate & Ecosystems Cooperative Research Centre, Hobart, Tasmania, ISBN 978-1-921197-05-5, 2010.

Hartstein, N. D., Maxey, J. D., Loo, J. C. H., and Then, A. Y. H.: Drivers of deep water renewal in Macquarie Harbour, Tasmania, J. Mar. Syst., 199, 103226, https://doi.org/10.1016/j.jmarsys.2019.103226, 2019.

Hashimoto, L. K., Kaplan, W. A., Wofsy, S. C., and McElroy, M. B.: Transformations of fixed nitrogen and N$_2$O in the Cariaco Trench, Deep-Sea Res. Part I, 30, 575–590, https://doi.org/10.1016/0198-0149(83)90037-7, 1983.

Hendzel, L. L., Matthews, C. J. D., Venkiteswaran, J. J., St. Louis, V. L., Burton, D., Joyce, E. M., and Bodaly, R. A.: Nitrous oxide fluxes in three experimental boreal forest reservoirs, Environ. Sci. Technol., 39, 4353–4360, https://doi.org/10.1021/es049443j, 2005.

Huang, Y., Song, B., Zhang, Q., Park, Y., Wilson, S. J., Tobias, C. R., and An, S.: Seawater intrusion effects on nitrogen cycling in the regulated Nakdong River Estuary, South Korea, Front. Mar. Sci., 11, 1369421, https://doi.org/10.3389/fmars.2024.1369421, 2024.

Inall, M. E. and Gillibrand, P. A.: The physics of mid-latitude fjords: a review, Geological Society, London, Special Publications, 344, 17–33, https://doi.org/10.1144/SP344.3, 2010.

Ji, Q., Jameson, B. D., Juniper, S. K., and Grundle, D. S.: Temporal and vertical oxygen gradients modulate nitrous oxide production in a seasonally anoxic fjord: Saanich Inlet, British Columbia, J. Geophys. Res.-Biogeo., 125, e2020JG005631, https://doi.org/10.1029/2020JG005631, 2020.

Kallert, J.: Verteilung von Lachgas (N$_2$O) und Methan (CH$_4$) im Fluss Rajang (Malaysia), Bachelor thesis, Christian-Albrecht-University, Kiel, https://oceanrep.geomar.de/id/eprint/40913/ (last access: 8 June 2023), 2017.

Ku, H. H.: Notes on the use of propagation of error formulas, J. Res. Nat. Bur. Stand., 70, https://doi.org/10.6028/jres.070C.025, 1966.

Kuypers, M. M. M., Marchant, H. K., and Kartal, B.: The microbial nitrogen-cycling network, Nat. Rev. Microb., 16, 263–276, https://doi.org/10.1038/nrmicro.2018.9, 2018.

Laffoley, D. and Baxter, J. M.: Ocean deoxygenation: Everyone's problem: Causes, impacts, consequences and solutions: Summary for Policy Makers, International Union for Conservation of Nature (IUCN), https://doi.org/10.2305/IUCN.CH.2019.13.en, 2019.

Li, Y., Yang, L., Jian, L., Wangwang, Y., Jiexia, Z., and Liyang, Z.: Sources and sinks of N$_2$O in the subtropical Jiulong River Estuary, Southeast China, Front. Mar. Sci., 10, 1138258, https://doi.org/10.3389/fmars.2023.1138258, 2023.

Limburg, K. E., Breitburg, D., Swaney, D. P., and Jacinto, G.: Ocean deoxygenation: A primer, One Earth 2, 24–29, https://doi.org/10.1016/j.oneear.2020.01.001, 2020.

Ma, X., Lennartz, S. T., and Bange, H. W.: A multi-year observation of nitrous oxide at the Boknis Eck Time Series Station in the Eckernförde Bay (southwestern Baltic Sea), Biogeosciences, 16, 4097–4111, https://doi.org/10.5194/bg-16-4097-2019, 2019.

Macquarie Harbour Dissolved Oxygen Working Group (October 2014), Final Report to the Tasmanian Salmonid Growers Association, 2014.

Maher, D. T., Sippo, J. Z., Tait, D. R., Holloway, C., and Santos, I. R.: Pristine mangrove creek waters are a sink of nitrous oxide, Sci. Rep., 6, 25701, https://doi.org/10.1038/srep25701, 2016.

Manning, C. C., Hamme, R. C., and Bourbonnais, A.: Impact of deep-water renewal events on fixed nitrogen loss from seasonally-anoxic Saanich Inlet, Mar. Chem., 122, 1–10, https://doi.org/10.1016/j.marchem.2010.08.002, 2010.

Maxey, J. D., Hartstein, N. D., Penjinus, D., and Kerroux, A.: Simple quality control technique to identify dissolved oxygen diffusion issues with biochemical oxygen demand bottle incubations, Borneo Journal of Marine Science and Aquaculture (BJoMSA), 1, 75–79 https://doi.org/10.51200/bjomsa.v1i0.995, 2017.

Maxey, J. D., Hartstein, N. D., Then, A. Y. H., and Barrenger, M.: Dissolved oxygen consumption in a fjord-like estuary, Macquarie Harbour, Tasmania, Estuar. Coast. Shelf Sci., 246, 107016, https://doi.org/10.1016/j.ecss.2020.107016, 2020.

Maxey, J. D., Hartstein, N. D., Mujahid, A., and Müller, M.: The influence of mesoscale climate drivers on hypoxia in a fjord-like deep coastal inlet and its potential implications regarding climate change: examining a decade of water quality data, Biogeosciences, 19, 3131–3150, https://doi.org/10.5194/bg-19-3131-2022, 2022.

McMahon, P. B. and Dennehy, K. F.: N$_2$O emissions from a nitrogen-enriched river, Environ. Sci. Technol., 33, 21–25, https://doi.org/10.1021/es980645n, 1999.

Michiels, C. C., Huggins, J. A., Giesbrecht, K. E., Spence, J. S., Simister, R. L., Varela, D. E., Hallam, S. J., and Crowe, S. A.: Rates and pathways of N$_2$ production in a persistently anoxic fjord: Saanich Inlet, British Columbia, Front. Mar. Sci., 6, 27, https://doi.org/10.3389/fmars.2019.00027, 2019.

Mickett, J. B., Gregg, M. C., and Seim, H. E.: Direct measurements of diapycnal mixing in a fjord reach–Puget Sound's Main Basin, Estuar. Coast. Shelf Sci., 59, 539–558, https://doi.org/10.1016/j.ecss.2003.10.009, 2004.

Murray, R., Erler, D. V., Rosentreter, J., Wells, N. S., and Eyre, B. D.: Seasonal and spatial controls on N$_2$O concentrations and emissions in low-nitrogen estuaries: Evidence from three tropical systems, Mar. Chem., 221, 103779, https://doi.org/10.1016/j.marchem.2020.103779, 2020.

Murray, R. H., Erler, D. V., and Eyre, B. D.: Nitrous oxide fluxes in estuarine environments: response to global change, Glob. Change Biol., 21, 3219–3245, https://doi.org/10.1111/gcb.12923, 2015.

Musenze, R. S., Werner, U., Grinham, A., Udy, J., and Yuan, Z.: Methane and nitrous oxide emissions from a subtropical estuary (the Brisbane River estuary, Australia), Sci. Total Environ., 472, 719–729, https://doi.org/10.1016/j.scitotenv.2013.11.085, 2014.

Mwanake, R. M., Gettel, G. M., Aho, K. S., Namwaya, D. W., Masese, F. O., Butterbach-Bahl, K., and Raymond, P. A.: Land Use, Not Stream Order, Controls N$_2$O Concentration and Flux in the Upper Mara River Basin, Kenya, J. Geophys. Res.-Biogeo., 124, 3491–3506, https://doi.org/10.1029/2019JG005063, 2019.

Myhre, G., Shindell, D., Bréon, F. M., Collins, W., Fuglestvedt, J., Huang, J., Koch, D., Lamarque, J. F., Lee, D., Mendoza, B., Nakajima, T., Robock, A., Stephens, G., Takemura, T., and Zhang, H.: Anthropogenic and Natural Radiative Forcing, in: Climate Change 2013: The Physical Science Basis, Contribution

of Working Group I to the Fifth Assessment Report of the Intergovernmental Panel on Climate Change, edited by: Stocker, T. F., Qin, D., Plattner, G. K., Tignor, M., Allen, S. K., Boschung, J, Nauels, A., Xia, Y., Bex, V., and Midgley, P. M., Cambridge University Press, Cambridge, United Kingdom and New York, NY, USA, https://doi.org/10.1017/CBO9781107415324.018, 2013.

Myllykangas, J.-P., Jilbert, T., Jakobs, G., Rehder, G., Werner, J., and Hietanen, S.: Effects of the 2014 major Baltic inflow on methane and nitrous oxide dynamics in the water column of the central Baltic Sea, Earth Syst. Dynam., 8, 817–826, https://doi.org/10.5194/esd-8-817-2017, 2017.

Nightingale, P. D., Malin, G., Law, C. S., Watson, A. J., Liss, P. S., Liddicoat, M. I., Boutin, J., and Upstill-Goddard, R. C.: In Situ Evaluation of Air-Sea Gas Exchange Parameterizations Using Novel Conservative and Volatile Tracers, Global Biogeochem. Cy., 14, 373–387, https://doi.org/10.1029/1999GB900091, 2000.

Orif, M. I., Yasar N. K., Radwan K. A., and Sudheesh, V.: Deoxygenation turns the coastal Red Sea lagoons into sources of nitrous oxide, Mar, Pollut, Bull., 189, 114806, https://doi.org/10.1016/j.marpolbul.2023.114806, 2023.

Osborn, T. R.: Estimates of The Local Rate of Vertical Diffusion from Dissipation Measurements, J. Phys. Oceanogr., 10, 83–89, https://doi.org/10.1175/1520-0485(1980)010<0083:EOTLRO>2.0.CO;2, 1980

Raes, E. J., Bodrossy, L., Van de Kamp, J., Holmes, B., Hardman-Mountford, N., Thompson, P. A., McInnes, A. S., and Waite, A. M.: Reduction of the powerful greenhouse gas N$_2$O in the South-Eastern Indian Ocean, PLoS One, 11, 1, https://doi.org/10.1371/journal.pone.0145996, 2016.

Raymond, P. A. and Cole, J. J.: Gas exchange in rivers and estuaries: Choosing a gas transfer velocity, Estuaries, 24, 312–317, https://doi.org/10.2307/1352954, 2001.

Reading, M. J.: Aquatic nitrous oxide dynamics from rivers to reefs, Doctoral dissertation, Southern Cross University, https://doi.org/10.25918/thesis.197, 2022.

Reading, M. J., Santos, I. R., Maher, D. T., Jeffrey, L. C., and Tait, D. R.: Shifting nitrous oxide source/sink behaviour in a subtropical estuary revealed by automated time series observations, Estuar. Coast. Shelf Sci., 194, 66–76, https://doi.org/10.1016/j.ecss.2017.05.017, 2017.

Reading, M. J., Tait, D. R., Maher, D. T., Jeffrey, L. C., Looman, A., Holloway, C., Shishaye, H. A., Barron, S., and Santos, I. R.: Land use drives nitrous oxide dynamics in estuaries on regional and global scales, Limnol. Oceanogr., 65, 1903–1920, https://doi.org/10.1002/lno.11426, 2020.

Resplandy, L., Hogikyan, A., Müller, J. D., Najjar, R. G., Bange, H. W., Bianchi, D., Weber, T., Cai, W.-J., Doney, S. C., Fennel, K., Gehlen, M., Hauck, J., Lacroix, F., Landschützer, P., Le Quéré, C., Roobaert, A., Schwinger, J., Berthet, S., Bopp, L., Chau, T. T. T., Dai, M., Gruber, N., Ilyina, T., Kock, A., Manizza, M., Lachkar, Z., Laruelle, G. G., Liao, E., Lima, I. D., Nissen, C., Rödenbeck, C., Séférian, R., Toyama, K., Tsujino, H., and Regnier, P.: A synthesis of global coastal ocean greenhouse gas fluxes, Global Biogeochem. Cy., 38, e2023GB007803, https://doi.org/10.1029/2023GB007803, 2024.

Robinson, A. D., Nedwell, D. B., Harrison, R. M., and Ogilvie, B. G.: Hypernutrified estuaries as sources of N$_2$O emission to the atmosphere: the estuary of the River Colne, Essex, UK, Mar. Ecol.

Prog. Ser., 164, 59–71, https://doi.org/10.3354/meps164059, 1998.

Rönner, U.: Distribution, production and consumption of nitrous oxide in the Baltic Sea, Geochim. Cosmochim. Ac., 47, 2179–2188, https://doi.org/10.1016/0016-7037(83)90041-8, 1983.

Rosentreter, J. A., Wells, N. S., Ulseth, A. J., and Eyre, B. D.: Divergent gas transfer velocities of CO$_2$, CH$_4$, and N$_2$O over spatial and temporal gradients in a subtropical estuary, J. Geophys. Res.-Biogeo., 126, e2021JG006270, https://doi.org/10.1029/2021JG006270, 2021.

Rosentreter, J. A., Laruelle, G. G., Bange, H. W., Bianchi, T. S., Busecke, J. J., Cai, W. J., Eyre, B. D., Forbrich, I., Kwon, E. Y., Maavara, T., and Moosdorf, N.: Coastal vegetation and estuaries are collectively a greenhouse gas sink, Nat. Clim. Change, 13, 579–587, https://doi.org/10.1038/s41558-023-01682-9, 2023.

Sánchez-Rodríguez, J., Sierra, A., Jiménez-López, D., Ortega, T., Gómez-Parra, A., and Forja, J.: Dynamic of CO$_2$, CH$_4$ and N$_2$O in the Guadalquivir estuary, Sci. Total Environ., 805, 150193, https://doi.org/10.1016/j.scitotenv.2021.150193, 2022.

Schulz, G., Sanders, T., Voynova, Y. G., Bange, H. W., and Dähnke, K.: Seasonal variability of nitrous oxide concentrations and emissions in a temperate estuary, Biogeosciences, 20, 3229–3247, https://doi.org/10.5194/bg-20-3229-2023, 2023.

Seitzinger, S. P., Kroeze, C., and Styles, R. V.: Global distribution of N$_2$O emissions from aquatic systems: natural emissions and anthropogenic effects, Chemosphere-Global Change Science, 2, 267–279, https://doi.org/10.1016/S1465-9972(00)00015-5, 2000.

Sierra, A., Jiménez-López, D., Ortega, T., Gómez-Parra, A., and Forja, J.: Factors controlling the variability and emissions of greenhouse gases (CO$_2$, CH$_4$ and N$_2$O) in three estuaries of the Southern Iberian Atlantic Basin during July 2017, Mar. Chem., 226, 103867, https://doi.org/10.1016/j.marchem.2020.103867, 2020.

Salamena, G. G., Whinney, J. C., Heron, S. F., and Ridd, P. V.: Internal tidal waves and deep-water renewal in a tropical fjord: Lessons from Ambon Bay, eastern Indonesia. Estuarine, Coast. Shelf Sc., 253, 107291, https://doi.org/10.1016/j.ecss.2021.107291, 2021.

Salamena, G. G., Whinney, J. C., Heron, S. F., and Ridd, P. V.: Frontogenesis and estuarine circulation at the shallow sill of a tropical fjord: Insights from Ambon Bay, eastern Indonesia, Regional Studies in Marine Science, 56, 102696, https://doi.org/10.1016/j.rsma.2022.102696, 2022.

Smith, R. W., Bianchi, T. S., Allison, M., Savage, C., and Galy, V.: High rates of organic carbon burial in fjord sediments globally, Nat. Geosci., 8, 450–453, https://doi.org/10.1038/ngeo2421, 2015.

Stow, C. A., Walker, J. T., Cardoch, L., Spence, P., and Geron, C.: N$_2$O emissions from streams in the Neuse River watershed, North Carolina, Environ. Sci. Technol., 39, 6999–7004, https://doi.org/10.1021/es0500355, 2005.

Sturm, K., Werner, U., Grinham, A., and Yuan, Z.: Tidal variability in methane and nitrous oxide emissions along a subtropical estuarine gradient, Estuar. Coast. Shelf Sci., 192, 159–169, https://doi.org/10.1016/j.ecss.2017.04.027, 2017.

Suntharalingam, P. and Sarmiento, J. L.: Factors governing the oceanic nitrous oxide distribution: Simulations with an ocean

general circulation model, Global Biogeochem. Cy., 14, 429–454, https://doi.org/10.1029/1999GB900032, 2000.

Tait, D. R., Maher, D. T., Wong, W., Santos, I. R., Sadat-Noori, M., Holloway, C., and Cook, P. L. M.: Greenhouse gas dynamics in a salt-wedge estuary revealed by high resolution cavity ringdown spectroscopy observations, Environ. Sci. Technol., 51, 13771–13778, https://doi.org/10.1021/acs.est.7b04627, 2017.

Tang, W., Talbott, J., Jones, T., and Ward, B. B.: Variable contribution of wastewater treatment plant effluents to downstream nitrous oxide concentrations and emissions, Biogeosciences, 21, 3239–3250, https://doi.org/10.5194/bg-21-3239-2024, 2024.

Teasdale, P. R., Apte, S. C., Ford, P. W., Batley, G. E., and Koehnken, L.: Geochemical cycling and speciation of copper in waters and sediments of Macquarie Harbour, Western Tasmania, Estuar. Coast. Shelf Sci., 57, 475–487, https://doi.org/10.1016/S0272-7714(02)00381-5, 2003.

Testa, J. M., Carstensen, J., Laurent, A., and Li, M.: Hypoxia and Climate Change in Estuaries, In Climate Change and Estuaries, 143–170, CRC Press, ISBN 9781003126096, 2023.

Tian, H., Xu, R., Canadell, J. G., Thompson, R. L., Winiwarter, W., Suntharalingam, P., Davidson, E. A., Ciais, P., Jackson, R. B., Janssens-Maenhout, G., Prather, M. J., Regnier, P., Pan, N., Pan, S., Peters, G. P., Shi, H., Tubiello, F. N., Zaehle, S., Zhou, F., Arneth, A., Battaglia, G., Berthet, S., Bopp, L., Bouwman, A. F., Buitenhuis, E. T., Chang, J., Chipperfield, M. P., Dangal, S. R. S., Dlugokencky, E., Elkins, J. W., Eyre, B. D., Fu, B., Hall, B., Ito, A., Joos, F., Krummel, P. B., Landolfi, A., Laruelle G. G., Lauerwald, R., Li, W., Lienert, S., Maavara, T., MacLeod, M., Millet, D. B., Olin, S., Patra, P. K., Prinn, R. G., Raymond, P. A., Ruiz, D. J., van der Werf, G. R., Vuichard, N., Wang, J., Weiss, R. F., Wells, K. C., Wilson, C., Yang, J., and Yao, Y.: A Comprehensive Quantification of Global Nitrous Oxide Sources and Sinks, Nature, 586, 248–256, https://doi.org/10.1038/s41586-020-2780-0, 2020.

Tian, H., Pan, N., Thompson, R. L., Canadell, J. G., Suntharalingam, P., Regnier, P., Davidson, E. A., Prather, M., Ciais, P., Muntean, M., Pan, S., Winiwarter, W., Zaehle, S., Zhou, F., Jackson, R. B., Bange, H. W., Berthet, S., Bian, Z., Bianchi, D., Bouwman, A. F., Buitenhuis, E. T., Dutton, G., Hu, M., Ito, A., Jain, A. K., Jeltsch-Thömmes, A., Joos, F., Kou-Giesbrecht, S., Krummel, P. B., Lan, X., Landolfi, A., Lauerwald, R., Li, Y., Lu, C., Maavara, T., Manizza, M., Millet, D. B., Mühle, J., Patra, P. K., Peters, G. P., Qin, X., Raymond, P., Resplandy, L., Rosentreter, J. A., Shi, H., Sun, Q., Tonina, D., Tubiello, F. N., van der Werf, G. R., Vuichard, N., Wang, J., Wells, K. C., Western, L. M., Wilson, C., Yang, J., Yao, Y., You, Y., and Zhu, Q.: Global nitrous oxide budget (1980–2020), Earth Syst. Sci. Data, 16, 2543–2604, https://doi.org/10.5194/essd-16-2543-2024, 2024.

Usui, T., Koike, I., and Ogura, N.: N$_2$O production, nitrification and denitrification in an estuarine sediment, Estuar. Coast. Shelf Sci., 52, 769–781, https://doi.org/10.1006/ecss.2000.0765, 2001.

Walinsky, S. E., Prahl, F. G., Mix, A. C., Finney, B. P., Jaeger, J. M., and Rosen, G. P.: Distribution and composition of organic matter in surface sediments of coastal Southeast Alaska, Cont. Shelf Res., 29, 1565–1579, https://doi.org/10.1016/j.csr.2009.04.006, 2009.

Walter, S., Bange, H. W., and Wallace, D. W.: Nitrous oxide in the surface layer of the tropical North Atlantic Ocean along a west to east transect, Geophys. Res. Lett., 31, L23S07, https://doi.org/10.1029/2004GL019937, 2004.

Walter, S., Breitenbach, U., Bange, H. W., Nausch, G., and Wallace, D. W. R.: Distribution of N$_2$O in the Baltic Sea during transition from anoxic to oxic conditions, Biogeosciences, 3, 557–570, https://doi.org/10.5194/bg-3-557-2006, 2006.

Wan, X. S., Lin, H., Ward, B. B., Kao, S., and Dai M.: Significant seasonal N$_2$O dynamics revealed by multi-year observations in the Northern South China Sea, Global Biogeochem. Cy., 36, e2022GB007333, https://doi.org/10.1029/2022GB007333, 2022.

Wan, X. S., Sheng, H. X., Liu, L., Shen, H., Tang, W., Zou, W., Xu, M. N., Zheng, Z., Tan, E., Chen, M., and Zhang, Y.: Particle-Associated Denitrification is the Primary Source of N$_2$O In Oxic Coastal Waters, Nat. Commun., 14, 8280, https://doi.org/10.1038/s41467-023-43997-3, 2023.

Wanninkhof, R.: Relationship Between Wind Speed and Gas Exchange Over the Ocean Revisited, Limnol. Oceanogr. Methods, 12, 351–362, https://doi.org/10.4319/lom.2014.12.351, 2014.

Weiss, R. F. and Price, B. A.: Nitrous oxide solubility in water and seawater, Mar. Chem., 8, 347–359, https://doi.org/10.1016/0304-4203(80)90024-9, 1980.

Wells, N. S., Maher, D. T., Erler, D. V., Hipsey, M., Rosentreter, J. A., and Eyre, B. D.: Estuaries as sources and sinks of N$_2$O across a land use gradient in subtropical Australia, Global Biogeochem. Cy., 32, 877–894, https://doi.org/10.1029/2017GB005826, 2018.

Willis, M.: TasCatch Variation 2 – Surface Water Models (Document ID Number WR 2008/005), Department of Primary Industries and Water, Hydro Tasmania Consulting, https://nre.tas.gov.au/Documents/Savage_TasCatch2_Report_Final1-1.pdf (last access: 1 November 2024), 2008.

Wilson, S. T., Bange, H. W., Arévalo-Martínez, D. L., Barnes, J., Borges, A. V., Brown, I., Bullister, J. L., Burgos, M., Capelle, D. W., Casso, M., de la Paz, M., Farías, L., Fenwick, L., Ferrón, S., Garcia, G., Glockzin, M., Karl, D. M., Kock, A., Laperriere, S., Law, C. S., Manning, C. C., Marriner, A., Myllykangas, J.-P., Pohlman, J. W., Rees, A. P., Santoro, A. E., Tortell, P. D., Upstill-Goddard, R. C., Wisegarver, D. P., Zhang, G.-L., and Rehder, G.: An intercomparison of oceanic methane and nitrous oxide measurements, Biogeosciences, 15, 5891–5907, https://doi.org/10.5194/bg-15-5891-2018, 2018.

Wilson, S. T., Al-Haj, A. N., Bourbonnais, A., Frey, C., Fulweiler, R. W., Kessler, J. D., Marchant, H. K., Milucka, J., Ray, N. E., Suntharalingam, P., Thornton, B. F., Upstill-Goddard, R. C., Weber, T. S., Arévalo-Martínez, D. L., Bange, H. W., Benway, H. M., Bianchi, D., Borges, A. V., Chang, B. X., Crill, P. M., del Valle, D. A., Farías, L., Joye, S. B., Kock, A., Labidi, J., Manning, C. C., Pohlman, J. W., Rehder, G., Sparrow, K. J., Tortell, P. D., Treude, T., Valentine, D. L., Ward, B. B., Yang, S., and Yurganov, L. N.: Ideas and perspectives: A strategic assessment of methane and nitrous oxide measurements in the marine environment, Biogeosciences, 17, 5809–5828, https://doi.org/10.5194/bg-17-5809-2020, 2020.

Wu, L., Chen X., Wei, W., Liu, Y., Wang, D., and Ni, B.: A critical review on nitrous oxide production by ammonia-oxidizing archaea, Environ. Sci. Technol., 54, 9175–9190, https://doi.org/10.1021/acs.est.0c03948, 2020.

Yevenes, M. A., Bello, E., Sanhueza-Guevara, S., and Farías, L.: Spatial distribution of nitrous oxide (N$_2$O) in the Reloncaví estuary–sound and adjacent sea (41–43 S), Chilean Patagonia, Estuar. Coast., 40, 807–821, https://doi.org/10.1007/s12237-016-0184-z, 2017.

Yoshinari, T.: Nitrous oxide in the sea, Mar. Chem., 2, 189–202, https://doi.org/10.1016/0304-4203(76)90007-4, 1976.

Zappa, C. J., Raymond, P. A., Terray, E. A., and McGillis, W. R.: Variation in surface turbulence and the gas transfer velocity over a tidal cycle in a macro-tidal estuary, Estuaries, 26, 1401–1415, https://doi.org/10.1007/BF02803649, 2003.

Zhang, G.-L., Zhang, J., Liu, S.-M., Ren, J.-L., and Zhao, Y.-C.: Nitrous oxide in the Changjiang (Yangtze River) Estuary and its adjacent marine area: Riverine input, sediment release and atmospheric fluxes, Biogeosciences, 7, 3505–3516, https://doi.org/10.5194/bg-7-3505-2010, 2010.

Zhang, W., Li, H., Xiao, Q., Jiang, S., and Li, X.: Surface nitrous oxide (N$_2$O) concentrations and fluxes from different rivers draining contrasting landscapes: Spatio-temporal variability, controls, and implications based on IPCC emission factor, Environ. Pollut., 263, 114457, https://doi.org/10.1016/j.envpol.2020.114457, 2020.